Project Title: Detection of Wildfires with Artificial Neural Networks

Project Team Members: John Leeman and Brent Umphlett

METR 4922 – Senior Seminar (Capstone) II

Project Number: 3

Mentor(s): Dr. Mark Morrissey, University of Oklahoma

Mentor Approval: _____

Date: May 3, 2011

Abstract

Currently fire detection using satellites is accomplished with algorithms and human analysts. Artificial neural networks (ANNs) have been shown to be more accurate than algorithms or statistical methods for applications dealing with multiple datasets of complex observed data in the natural sciences (Hsieh and Tang, 1998). This paper presents results from the testing of an ANN in detecting wildfires utilizing polar orbiter numerical data from the Advanced Very High Resolution Radiometer (AVHRR). Datasets containing locations of known fires were gathered from the National Oceanic and Atmospheric Administration's (NOAA) polar orbiting satellites via the Comprehensive Large Array-data Stewardship System (CLASS). The data was then calibrated and navigation corrected using the Environment for Visualizing Images (ENVI). Fires were located with the aid of shapefiles generated via ArcGIS. Afterwards, smaller ten pixel by ten pixel datasets were created, which contained the fire (using the ENVI corrected data). To vary fire positions in these smaller images, several images of the same fire were created, each with the fire in a different location. This ensured that the ANN did not only handle cases where the fire was in the center of the image, which is needed for this methodology to be applied operationally. Datasets containing no fires were also created. These smaller datasets were then randomly separated into categories used to train, validate, and test the ANN. To prevent overtraining of the ANN the mean squared error (MSE) of the network was monitored and training was stopped when the MSE began to rise. The accuracy of the neural network was then statistically evaluated. The most accurate fire classification network used all six bands of AVHRR data to achieve an accuracy ranging from 73-90%.

1. Introduction

1.1 Motivation

Wildfire detection is necessary for accurate record keeping, fire management, and even large fire detection in rural areas. Wildfires destroyed an estimated 15 x 10^6 km^2 of forest in the decade before 1993 (Singh, 1993). In addition, atmospheric modelers struggle with wildfires because they can alter local atmospheric chemistry; in some areas fire is the dominant carbon release mechanism, making it vital to closing the carbon balance (Sellers et al., 1995).

1.2 Previous Research

Remote detection of wildfires has been attempted with a variety of techniques and data products with mixed success. Difficulty in verifying fire location, making a computationally reasonable algorithm, and quality control all make this a difficult problem in the remote sensing community.

Detection of wildfire smoke was investigated with limited success by Li et al. (2001) using both neural network and multi-threshold approaches. While neural networks provided the desired learning capability they were slow to train over large spatial domains. Multi-threshold approaches did not suffer from processing limitations, but the simple categorized output was not as useful and both methods suffered when applied to a very large geographic region.

The satellite services division (SSD) has also experimented using nighttime visible imagery to detect fires. After removing the known lighting sources, an analyst can determine if residual light areas on the plot are the product of a fire or an uncorrected

anthropogenic source. The method is very susceptible to cloud cover and still requires much human input (McNamara et al., 2002).

A multi-institution team headed by Jerry Miller of the National Aeronautics and Space Administration (NASA) completed a project utilizing three bands of data from Geostationary Operational Environmental Satellite (GOES), the Advanced Very High Resolution Radiometer (AVHRR), and the Moderate Resolution Imaging Spectroradiometer (MODIS). Miller et al. determined that they saw no unique signature for different fire types such as a ground or crown fire in their data.

The current fire product from the National Oceanic and Atmospheric Association (NOAA) uses a combination of many algorithms and human skill to accurately mark locations of wildfires. Information from MODIS, AVHRR, and GOES is used for the product. Once data is received from a satellite, it is put through an algorithm for that respective satellite. The Wildfire Automated Biomass Burning Algorithm (WF-ABBA) is used on GOES data, the Fire Identification, Mapping and Monitoring Algorithm (FIMMA) is used on AVHRR data, and MODIS has it's own specific algorithm. After viewing algorithm output and raw satellite images the analyst quality controls the products before they are released by marking fires the algorithms have missed and deleting false positives.

1.2 Use of Artificial Neural Networks

Neural networks, similar to the human brain, are classification machines. In a basic case the network learns classification from a set of exemplars used to train the network. After training, the network can be used to classify unknown data. The simple model for a neural network was proposed in the 1950's and independently developed

(Rosenblatt, 1958; Widrow and Sterns, 1985). Early neural networks were deemed as poor classifiers (Minsky and Papert, 1969) until the 1980's when interest in neural network classification surged after the development of back propagation algorithms through hidden neuron layers.

In both the brain and a neural network there are many interconnected neurons. Each connection between two neurons is assigned a weight, defined as the strength of interaction/influence of the neurons on each other. According to Hebb's rule, the more the two neurons fire together (strong correlation) the heavier their connection will be weighted. Modified and mathematically elegant implementations of this idea have been developed and implemented into modern ANN design.

Significant evidence exists (Benediktsson et al., 1990) that neural networks can out perform statistical methods with remote sensing data. Neural networks have been compared to statistical methods of classification for remote sensing data from multiple sources, and it has been found that neural networks have the advantage when no prior knowledge about the statistical distribution of classes in the data sources is available. Neural networks also handle multi-source data sets well, in which all data sources may not be equally reliable (a difficult problem in many statistical frameworks). This project was meant to evaluate the efficiency and accuracy of using ANNs to detect fires from AVHRR satellite imagery, and thus determine if ANNs could possibly be used in the future along with current algorithms, or possibly on their own, to improve accuracy of remote wildfire detection.

2. Details and Methods

2.1 Data Acquisition

The first step in data acquisition was determining the times and locations of wildfires that had occurred. To determine times and locations of wildfires, an internet search for news articles about wildfires was conducted. National Weather Service graphics from wildfire outbreaks in Oklahoma were incorporated as well. The approximate start and end times, approximate location, and approximate size in acres of these wildfires were recorded.

Once times and locations of wildfires were known, satellite images including these times and locations were downloaded from NOAA's Comprehensive Large Array-data Stewardship System (CLASS). These images were opened in the Environment for Viewing Images (ENVI) and guidance corrected, accounting for satellite navigation error. Once guidance corrected, fires located in the images were numbered. Then, using ENVI, one to four ten by ten pixel data sets were created for each fire, varying the position of the fire in each image. This method yielded a larger and more varied fire database to be used later when utilizing the ANN. Varying fire position was also done to prevent the ANN from training to detect fires in the same spot in each image. Each ten by ten section was exported to a text file that contained the numerical values for all six channels measured by the AVHRR.

In order to train the ANN properly both "fire" images and "no-fire" images were needed. This helps ensure that the network will train on what is wanted, not an unforeseen factor in the data. Overall 259 "no-fire" cases were stored and 346 "fire" cases were stored for a total of 605 cases for the network to train, validate, and test on.

2.2 Data Analysis using ANNs

Most neural networks can be generalized in the form shown in figure 1. Input data are sent to the input layer as vectors and then propagated through connections to the hidden and output layers. The weight of each connection is determined during training of the network. To train the network, it is shown examples of input vectors and the desired output vectors. Weights are adjusted through various training algorithms and then the network is validated and tested. The training algorithms are non-trivial in nature and are further discussed in Hagan et al., 2002. Training is conducted until the neural activation energies and connection weights are believed to be most accurate, which is referred to as well fit. Over or under training (fitting) can reduce the classification efficiency of the neural network.

The MATLAB neural network toolbox network pattern recognition tool (nprtool) was used to initialize the network and a MATLAB code was exported. The files produced by ENVI were formed into comma delimited files with a simple Python script containing all input and output vectors. Several files were produced containing each AVHRR channel individually, channels 3a and 3b combined, and all six channels combined. This resulted in eight datasets to work with. The data was randomly divided into training, testing, and validation sub-sets with 65% for training, 15% for validation, and 20% for testing. The network was trained on the input vectors in the training set.

Training was accomplished with the scaled conjugate descent algorithm (SCG). This algorithm was chosen for its computational speed. Levenberg-Marquardt training proved to be unacceptably slow with this data set. Conjugate gradient algorithms are also common in neural networks. Basic back propagation training techniques descend the

error surface in the steepest descent direction (highest negative gradient of the error surface). While this does work, it is not always the most efficient path to solution convergence. Conjugate gradient algorithms search along conjugate paths, but this still requires a line search with increases the computational workload. The SCG prevents the need for this line search by pulling ideas from Levenberg-Marquardt. For a detailed discussion of the mathematics see (Moller, 1993).

Validation is an important step to insure the network is not over fit (has fit the noise in the data, not the general trend). Over fitting is illustrated in figure 2 and can be thought of as using a high degree polynomial on a simple data set, fitting every point of data. To prevent over fitting of data the mean squared error is monitored and upon increasing, training is halted.

After validation the network is shown data it has to this point not been exposed to, the testing sub-set. Error in classification on the testing sub-set is recorded as total error, true positives, false positives, true negatives, and false negatives. These figures are likely representative of how the network may preform in an operational setting neglecting a few problems such as breaks in the clouds, cloud cover obscuring the fire, or sun-glint (no examples of these cases were included in the data).

The process of dividing the data randomly, training, validating, and testing was carried out 10 times for each network configuration (number of hidden layer neurons, and AVHRR channels used for input). The number of hidden layer neurons was varied from five to three hundred fifty in increments of five. This results in 552 network configurations to be evaluated.

3. Results and Discussion

Figures F1-F8 show the total confusion matrix parameters for each individual channel tested as well as the two combinations of channels tested. A confusion matrix plots the percentage of true positives, true negatives, false positives, and false negatives output by the ANN. Total, in this case, means that the parameters are summarized for all the data subsets (training, validation, and testing). The higher the percentage of positive classifications, and thus the lower the percentage of false classifications, the better the performance of the ANN. The performance of channel 3a (figure F3) was similar to that of 3b (figure F4), but the combination of the two (figure F7) shows a reduction in scatter and a slightly raised true negative rate. Channel 1 (figure F1) demonstrated a high false positive rate; channel 2 (figure F2) exhibited similar results. Channels 4 (figure F5) and 5 (figure F6) were better than channels 1 and 2 when determining true negatives. The lowest scatter and most desirable result was obtained with all six channels (figure F8).

Figures 3 and 4 are two different views of the same plot that summarize the performance of the ANN. Error (false classification) displayed is only error on the test dataset, data the network was only exposed to once for testing to evaluate real-life expected output in which new situations are encountered. Channels 1 and 2 were clearly the least accurate, and the combination of 3a and 3b was more accurate than either alone. The highest accuracy (73%-90%) was achieved by using all channels of the instrument.

Figure 5 shows the test set error when utilizing all bands of data from the AVHRR. It is a 2D plot of the "All" data set in figures 3 and 4. This test set error shows little improvement with increasing hidden layer neurons. There seem to be two weak minima around 125 and 240 neurons. The fewer neurons are desirable to reduce

computation time. With a more robust and larger data set the effect of hidden layer neurons may become clearer.

Figure 6 is a plot of the number of training epochs (passes through the data) as a function of input channels and number of hidden layer neurons. This figure shows that the number of training epochs exhibits little dependence on the number of hidden layer neurons. There is a general increasing trend as more complex data is utilized, but the computational demands are within reason.

Fires that occur on the ground (especially in the early stages of fire development) may be covered by a heavy forest canopy, which may significantly hamper detection. Sun glint off bodies of water has also been noted as a significant cause of false positives (Setzer and Malingreau, 1996). Areas in which local surface temperature is high may present a decreased contrast between the land surface and the fire making the detection much more difficult and less certain, though it has been suggested that fire smoke can induce surface cooling (Robuck, 1991). Cloud cover can mask evidence of a fire on the surface, exemplified by Li et al. (2000). Neural network limitations will somewhat hamper the efforts to detect fire. Hsieh and Tang (1998) discussed the difficulties of applying neural networks to meteorological and oceanographic data sets. The main points were: non-linear instability with short data records, dealing with large spatial fields, and difficulties of interpreting the non-linear outputs of a neural network. The determination was that all three issues could be addressed with ensemble averaging/pruning and non-convergent methods, data pre-filtering through principle component analysis (PCA), and interpreting the network hidden layer in a phase space

framework respectively. Since the wildfire detection problem considers complex multi-type, multi-source data, neural networks appear to be the optimal tool.

4. Conclusions and Summary

The most accurate fire classification network used all six bands of AVHRR data to achieve an accuracy ranging from 73-90%. This variability is due to the random training of the network and random division of data into training, test, and validation data subsets. Based on these results, neural networks have a place in a future suite of remote fire detection tools. Even with an accurate network, some human oversight is necessary to ensure quality detections.

Comparison of the 73-90% network accuracy with current algorithms is not possible as this network accuracy was determined with a limited number of cases. Scanning multiple satellite images with neural network and algorithmic methods, and then comparing the results would yield a better comparison. A combination of neural networks and algorithms is likely the most effective operational combination. With the current dataset a network with ~125 hidden neurons and a 600 element input vector using all 6 channels of the AVHRR data is likely the best configuration.

Further work to improve the accuracy of ANN fire classification could focus on using higher resolution satellite data, utilizing multiple satellite sources such as GOES and MODIS, utilizing radar imagery (especially dual polarization radar) to look for smoke plumes, including fire risk parameters to prioritize image scanning, and determining diurnal and seasonal accuracy variations. It may also be useful to determine a fire size detection threshold, improve filtering of anthropogenic signatures such as power stations, and investigate time series prediction of fire evolution.

5. References

Benediktsson, J.A., Swain, P.H., and Ersoy, O.K., 1990: Neural Network Approaches Versus Statistical Methods in Classification of Multisource Remote Sensing Data. IEEE Tran. On Geoscience and Remote Sensing, 28, 540-552.

Hagan, M.T., Demuth, H.B., and Beale, M.H., 2002: Neural Network Design. Colorado University Bookstore.

Hsieh, W.W., Tang, B., 1998: Applying Neural Network Models to Prediction and Data Analysis in Meteorology and Oceanography. Bulletin of the American Meteorological Society, 79, 1855-1970.

Li, Z., Khananian, A., Fraser, R.H., and Cihlar, J., 2001: Automatic Detection of Fire Smoke Using Artificial Neural Networks and Threshold Approaches Applied to AHVRR Imagery. IEEE Trans. on Geoscience and Remote Sensing, 39, 1859-1970.

Li, Z., Nadon, A., Cihlar, J., 2000: Satellite-based detection of Canadian boreal forest fires: development and application of the algorithm. Int. J. of Remote Sensing, 16, 3057-3069.

McNamara, D., Stephens, G., and Ruminiski, M., 2002: NOAA's multi-sensor fire detection program using environmental satellites. Earth System Monitor, 13, 1-7.

Miller, J., Borne, K., Zhenping, H., and Chi, Y.: Automated Wildfire Detection through Artificial Neural Networks. NASA.

Minsky, M., and Papert, S., 1969: Perceptrons. MIT Press, 292 pp.

Moller, M.F., 1993: A Scaled Conjugate Gradient Algorithm for Fast Supervised Learning. Neural Networks, 6, 525-533.

Robock, A., 1991: Surface Cooling Due to Forest Fire Smoke. Journal of Geophysical Research, 96, 20869-20878.

Rosenblatt, F., 1958: The Perceptron: A Probabilistic Model for Information Storage and Organization in the Brain. Psychological Review, 65, 386-408.

Sellers, P.J., Hall, F.G., Margolis, H., Kelly, B., Baldocchi, D., DenHartog, J., Chilar, J., Ryan, M., Goodison, B., Crill, P., Ranson, J., Lettenmaier, D., and Wickland, D.E. 1995: The Boreal Ecosystem-Atmospheric Study (BOREAS): an overview and early results from 1995 field year. Buletin of American Meteorological Society, 76, 1549-1577.

Setzer, A.W., and Malingreau, J.P., 1996, AVHRR monitoring of vegetation fires in the tropics: toward the development of a global product. Biomass Burning and Global Change, 25-39.

Singh, K.D., 1993: The 1990 tropical forest resource assessment, Unasyva/FAO, 44, 10-19.

Widrow, B., and Sterns, S.D.: Adaptive Signal Processing. Prentice-Hall, 474pp.

Figures

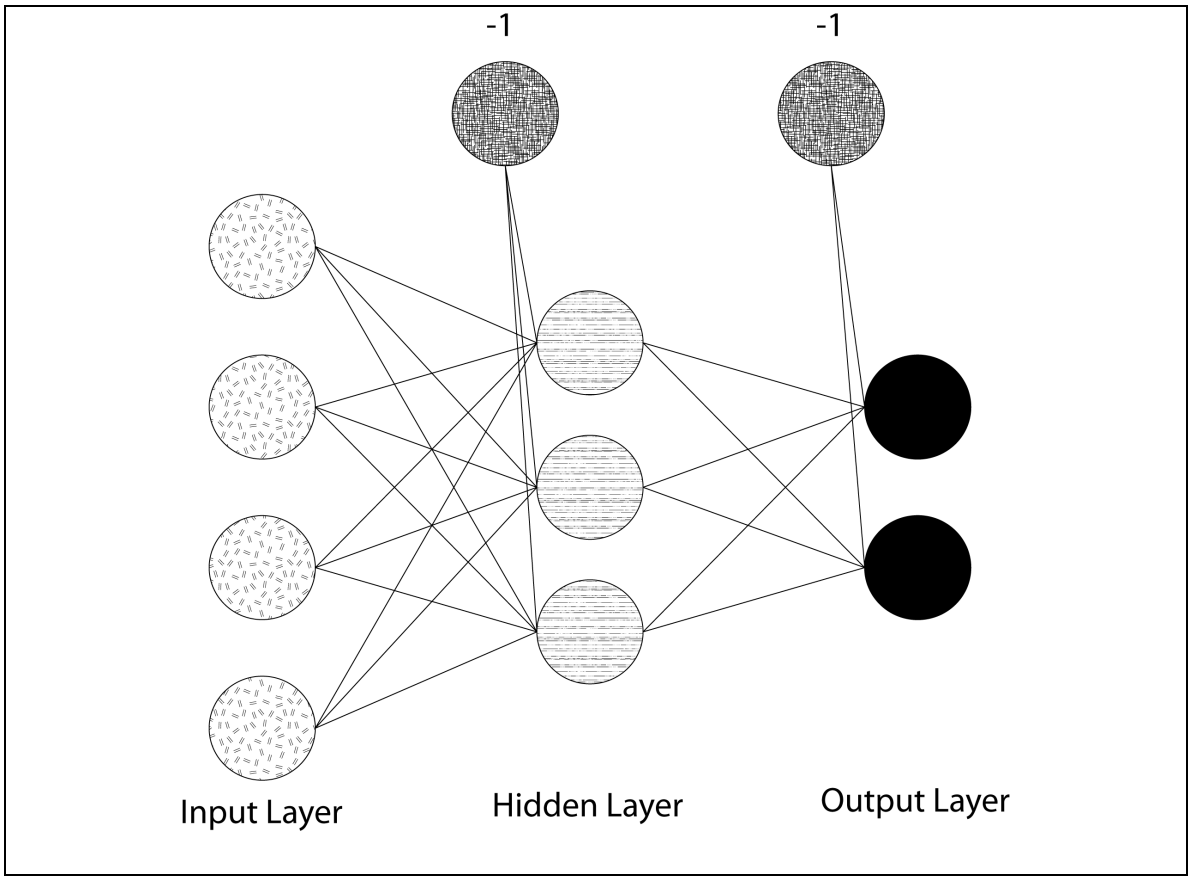

Figure 1- The basic layout of a neural network with one hidden layer. The input vectors are fed into the system on the left hand side, and processed to produce the output activations on the right hand side. The -1 constant nodes are bias nodes.

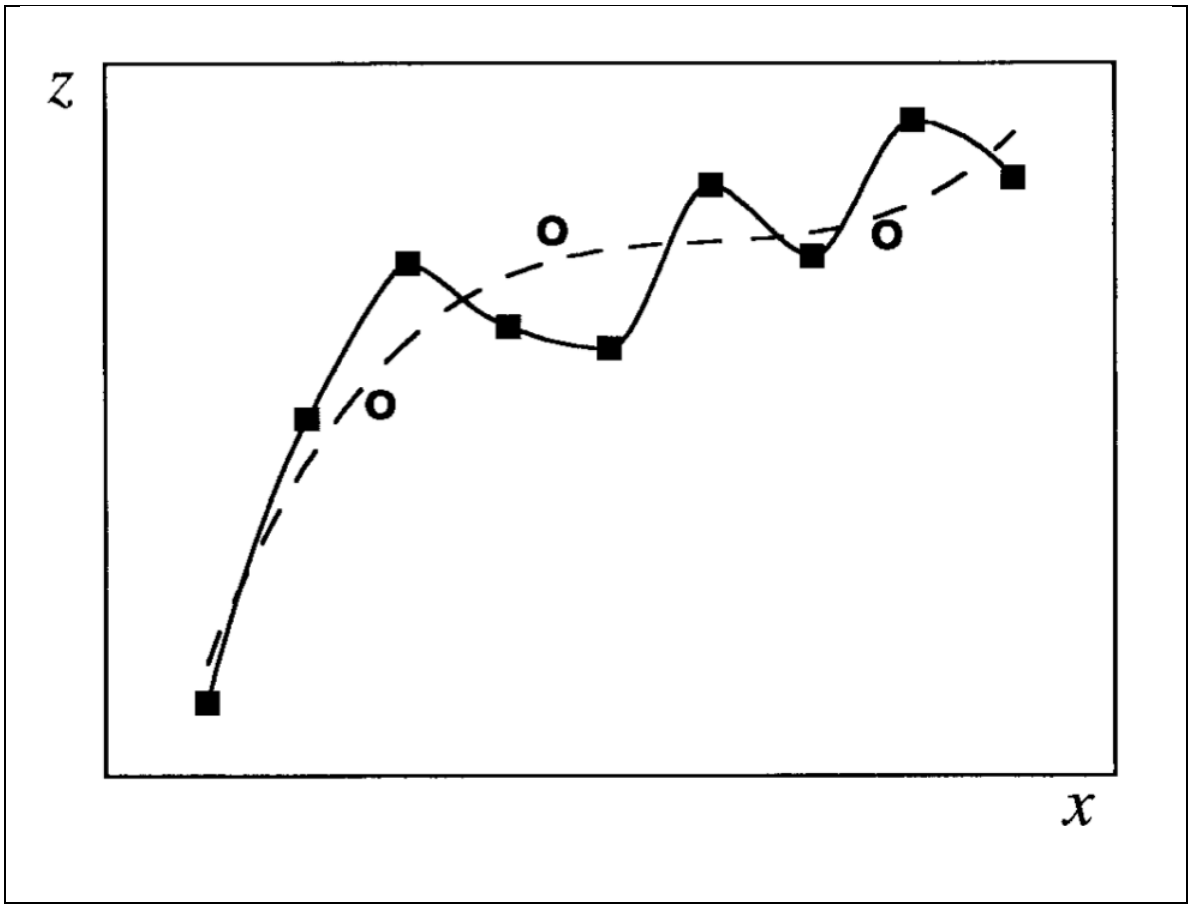

Figure 2- A demonstration of over fitting. The solid line represents the fitting of noise in the data, while the dashed line shows the output of a properly trained neural network, which fits the general trend of the data. (Hsieh and Tang, 1998)

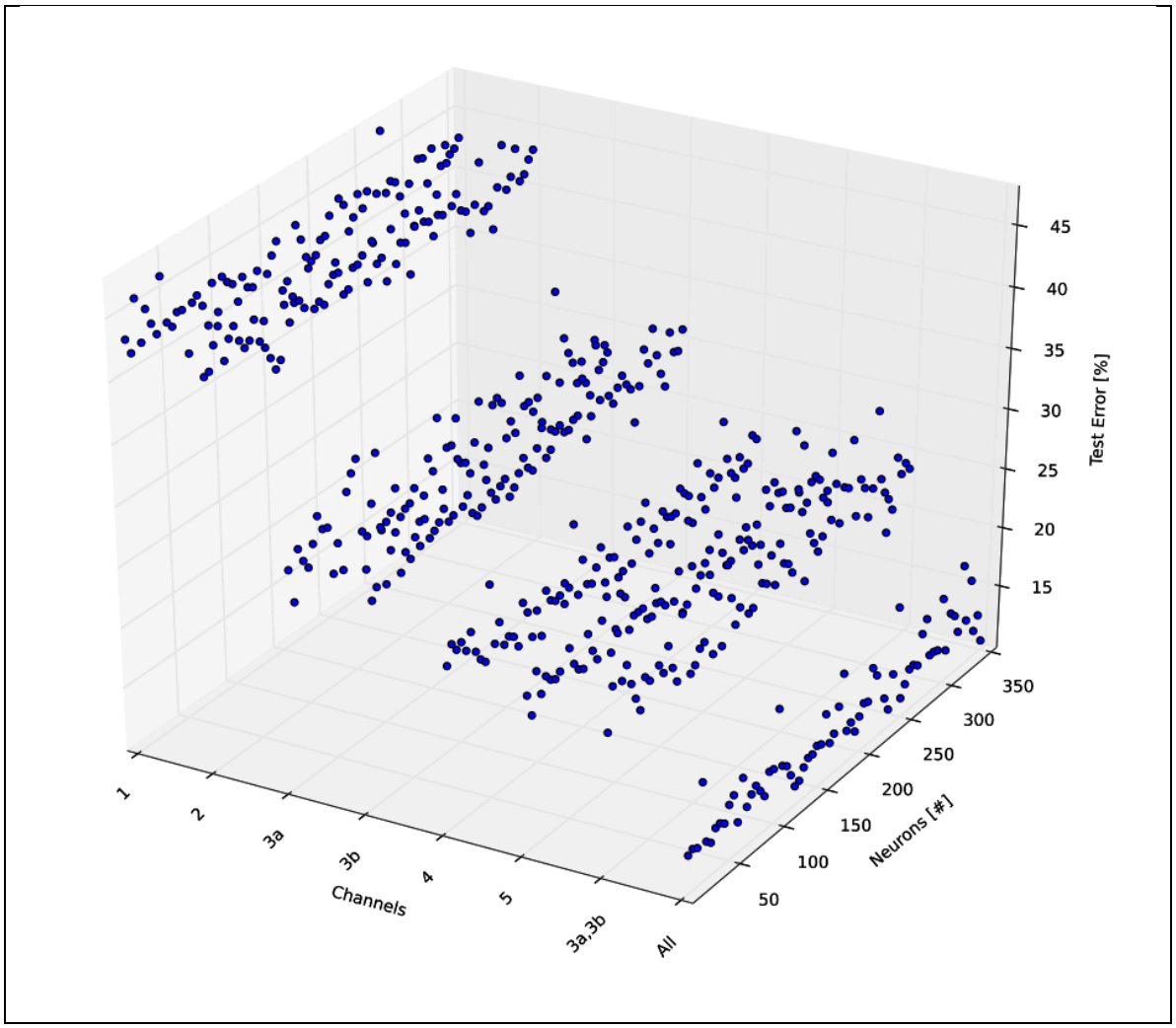

Figure 3 – A view of the error associated with the test data sub-set as a function of the number of hidden neurons and the channels of AVHRR data used. It is clear that using all channels produces the best results with little variation due to the number of hidden layer neurons. A profile of the error as a function of number of neurons is given in figure 6.

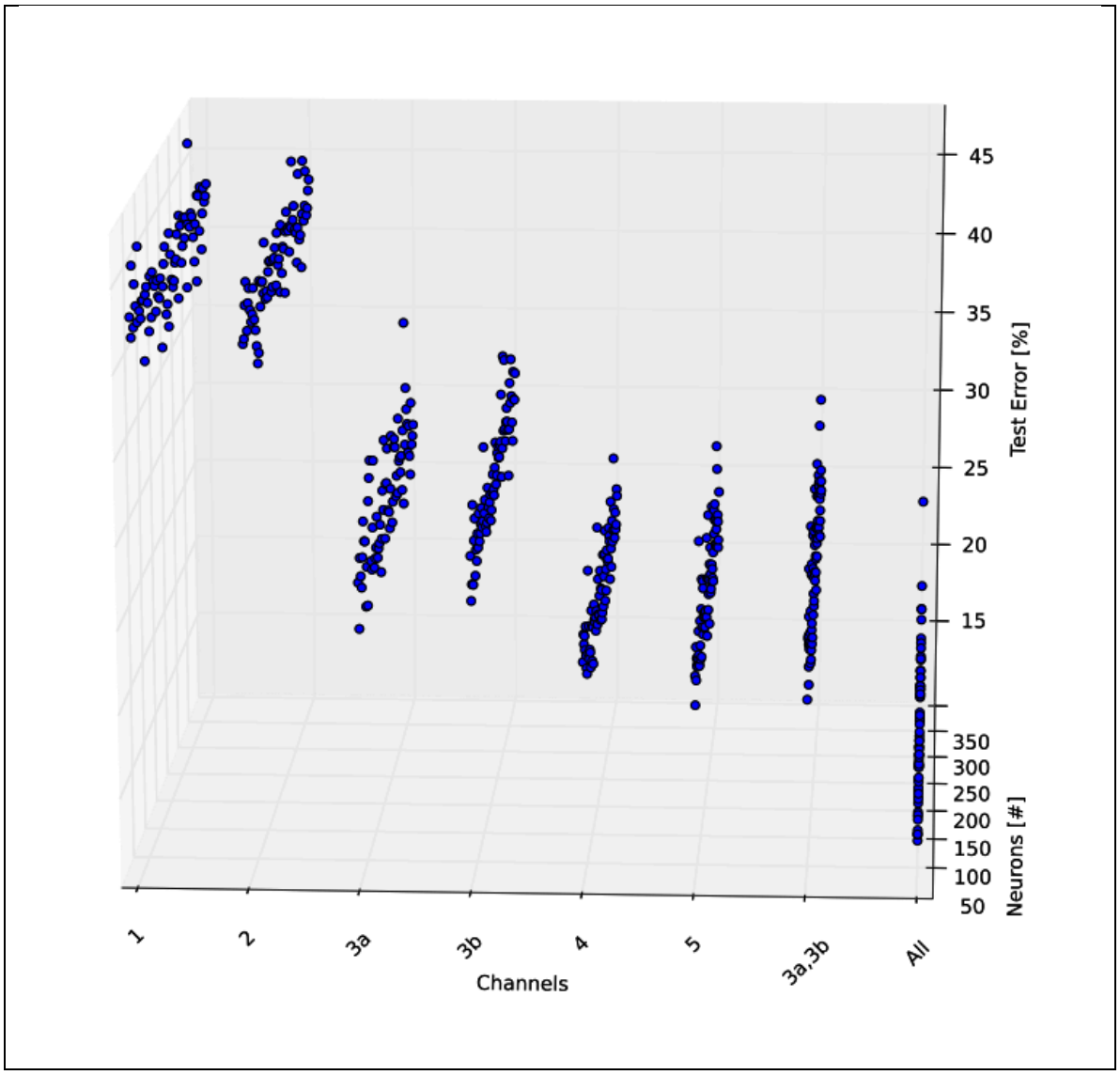

Figure 4 – A second view of the error associated with the test data sub-set as a function of the number of hidden neurons and the channels of AVHRR data used (as in figure 3). This view makes it easier to determine which channels, in general, had the lowest error. As expected IR and near-IR channels have lower error than any other individual channel.

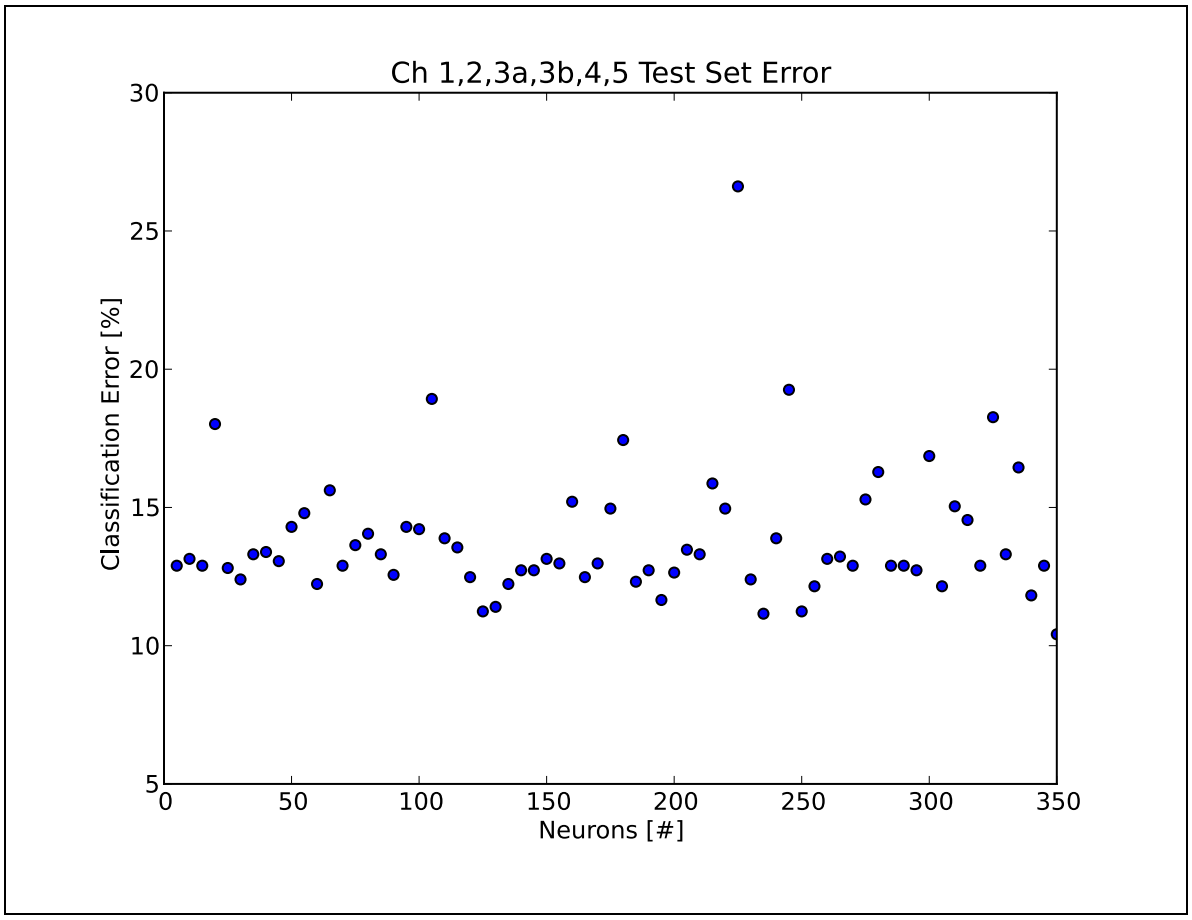

Figure 5 - Test set error when utilizing all bands of data from the AVHRR shows little improvement with increasing hidden layer neurons. There seem to be two weak minima around 125 and 240 neurons. The fewer neurons are desirable to reduce computation time.

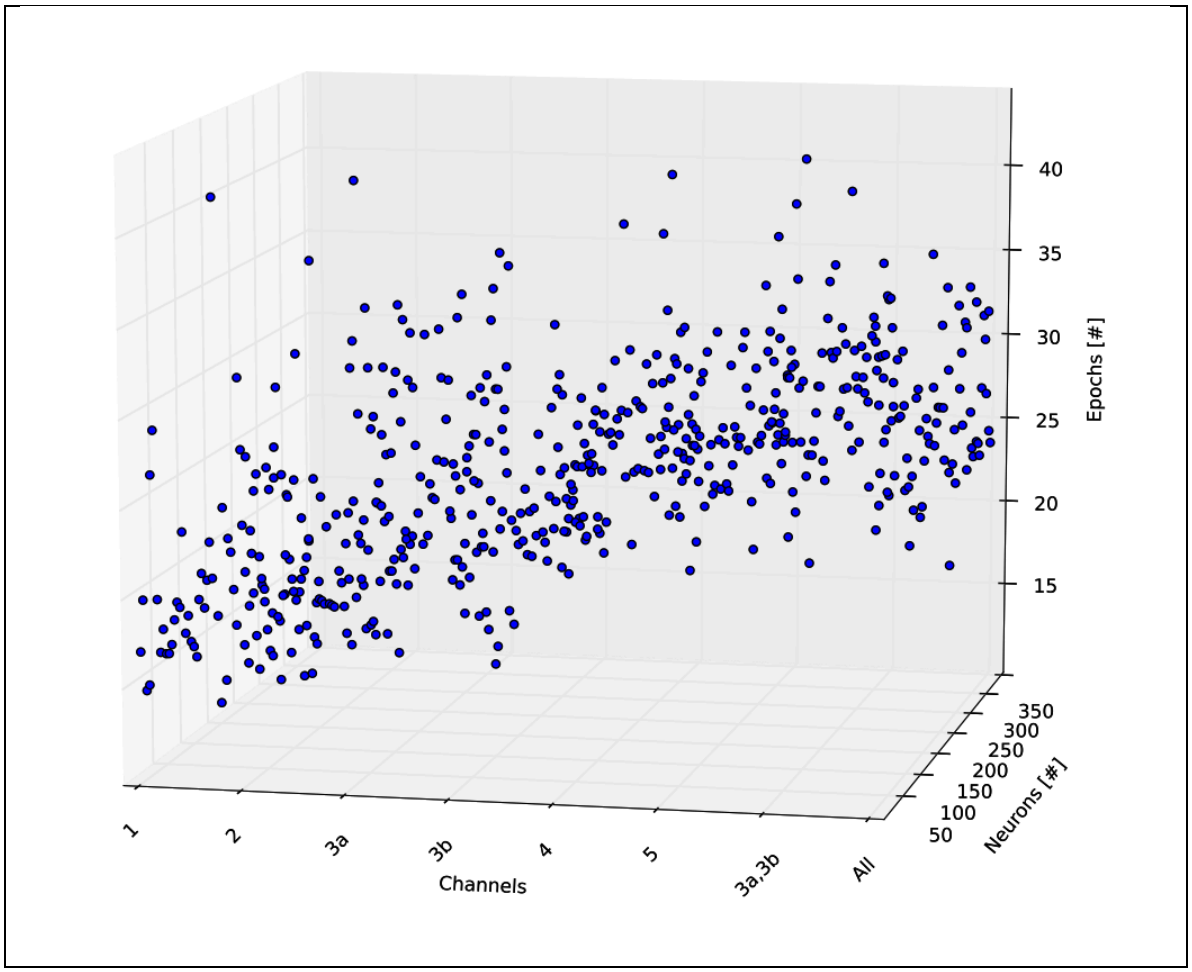

Figure 6 - The number of training epochs as a function of input channels and number of hidden layer neurons exhibits little dependence on the number of hidden layer neurons. There is a general increasing trend as more complex data is utilized, but the computational demands are within reason.

6. Appendices

Appendix A – Total Classification Error Plots

The following plots summarize classification error (false positive or false negative) for the training, test, and validation data sub-sets. Results for each channel combination are presented.

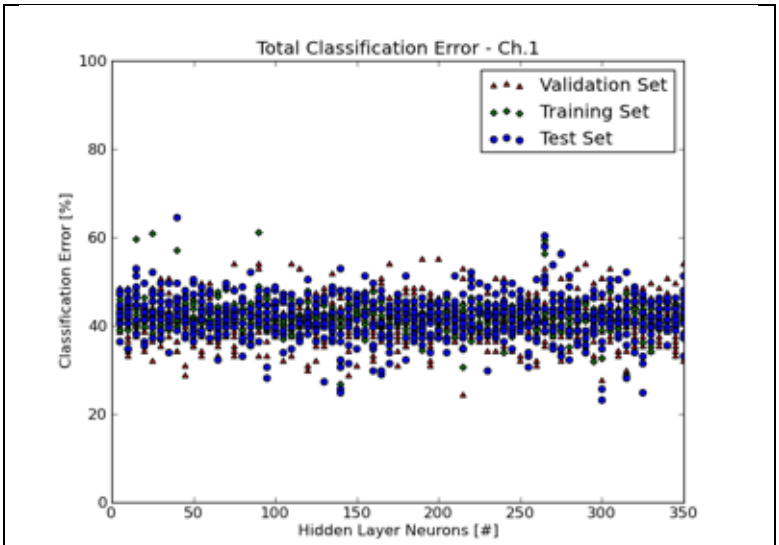

Figure A1 – Classification error on all data sub-sets utilizing Ch.1 of the AVHRR data.

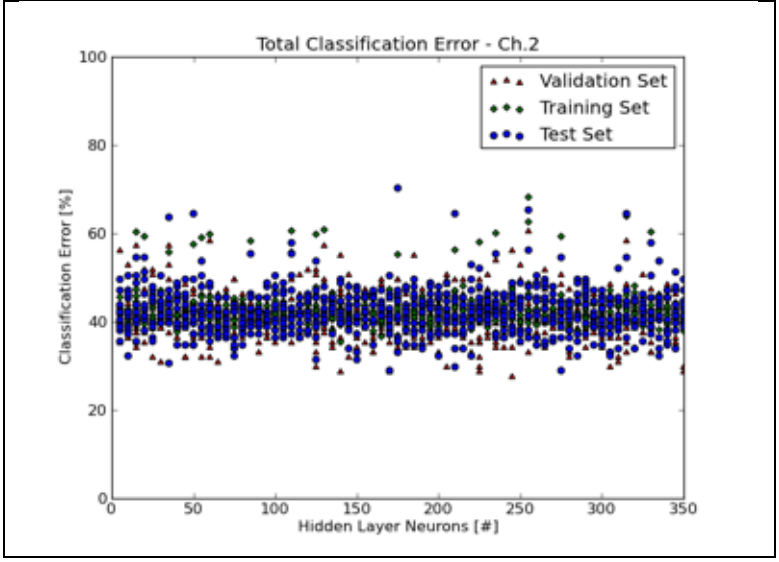

Figure A2 – Classification error on all data sub-sets utilizing Ch.2 of the AVHRR data.

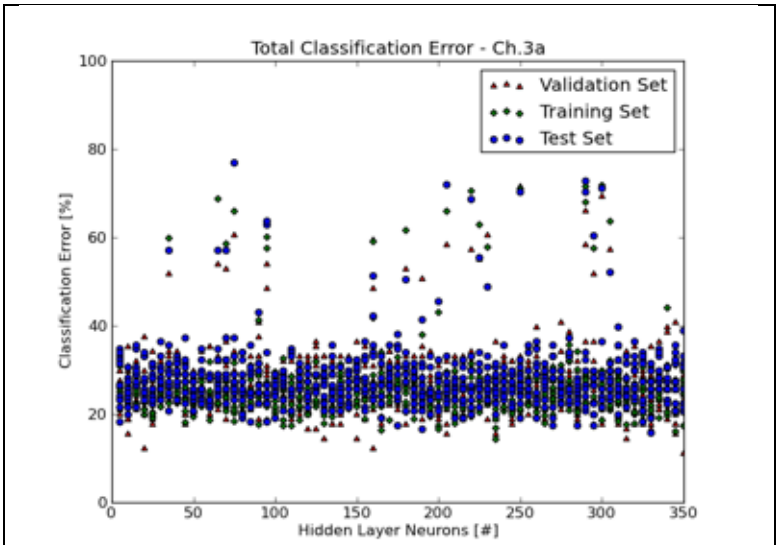

Figure A3 – Classification error on all data sub-sets utilizing Ch.3a of the AVHRR data.

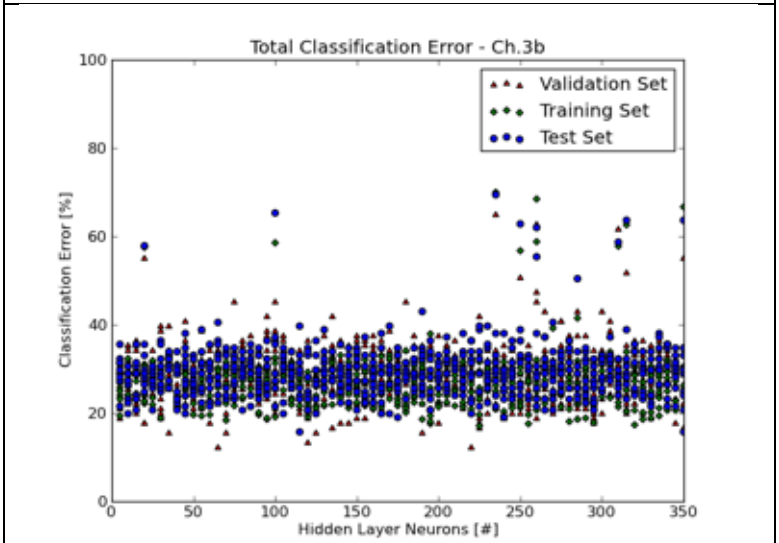

Figure A4 – Classification error on all data sub-sets utilizing Ch.3b of the AVHRR data.

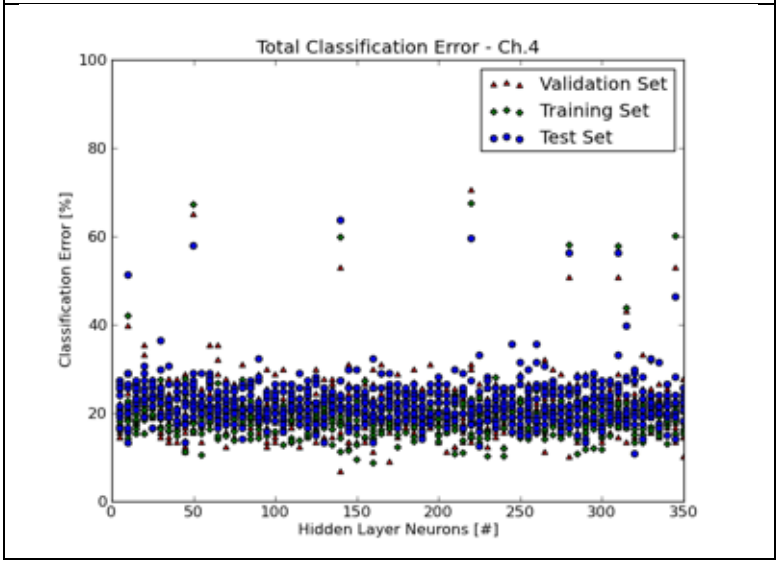

Figure A5 – Classification error on all data sub-sets utilizing Ch.4 of the AVHRR data.

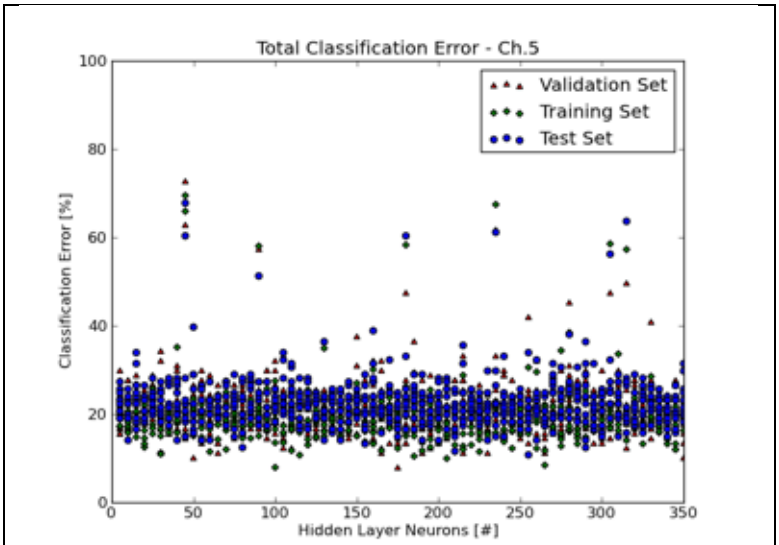

Figure A6 – Classification error on all data sub-sets utilizing Ch.5 of the AVHRR data.

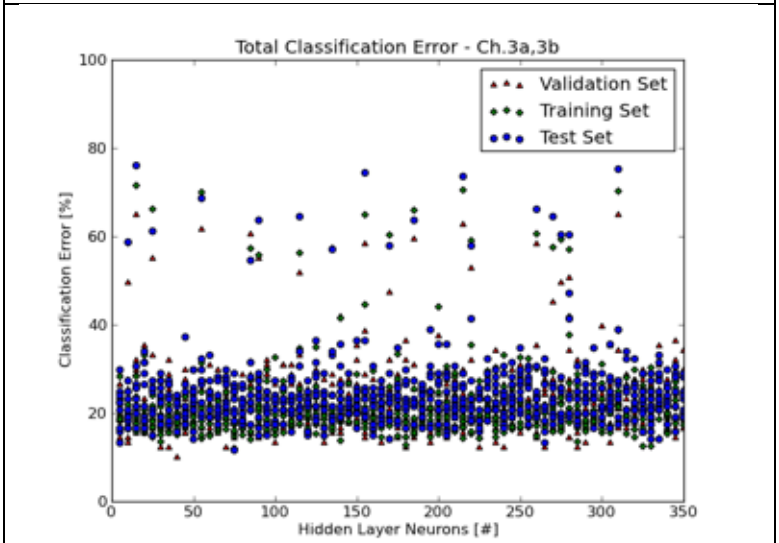

Figure A7 – Classification error on all data sub-sets utilizing Ch.3a,3b of the AVHRR data.

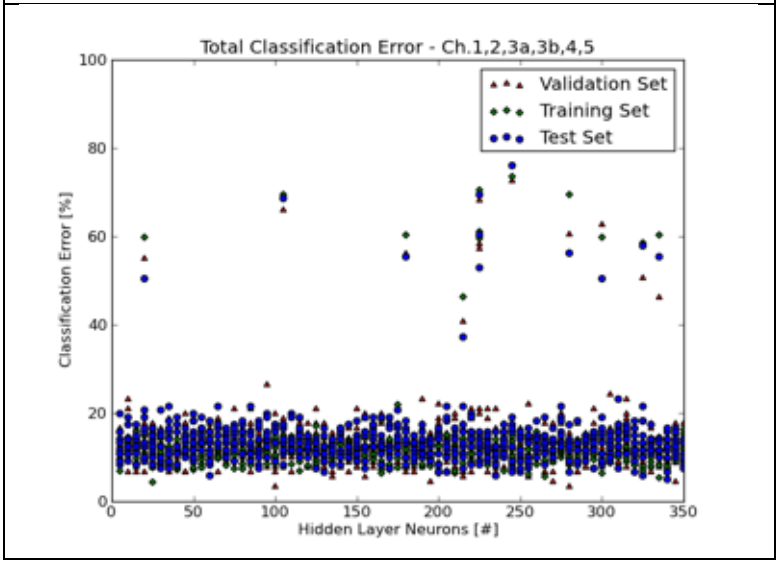

Figure A8 – Classification error on all data sub-sets utilizing all channels of the AVHRR data.

Appendix B – Training Epoch Plots

The following plots summarize the number of training epochs (passes through the data) required to train the network. Results for each channel combination are presented.

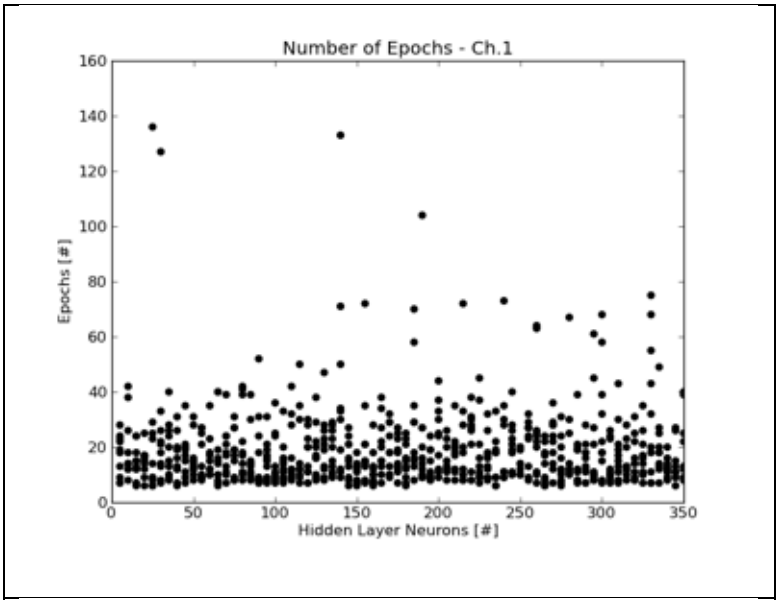

Figure B1 – Number of training epochs required using AVHRR data from Ch.1.

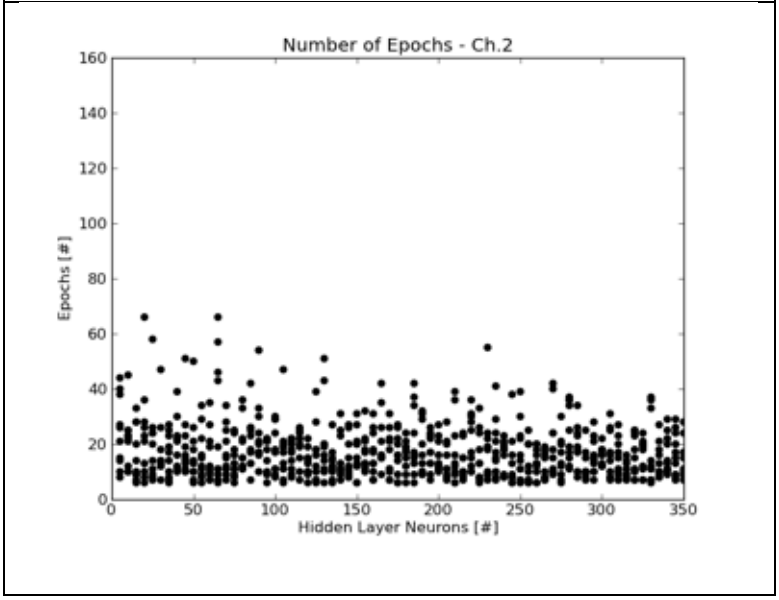

Figure B2 – Number of training epochs required using AVHRR data from Ch.2.

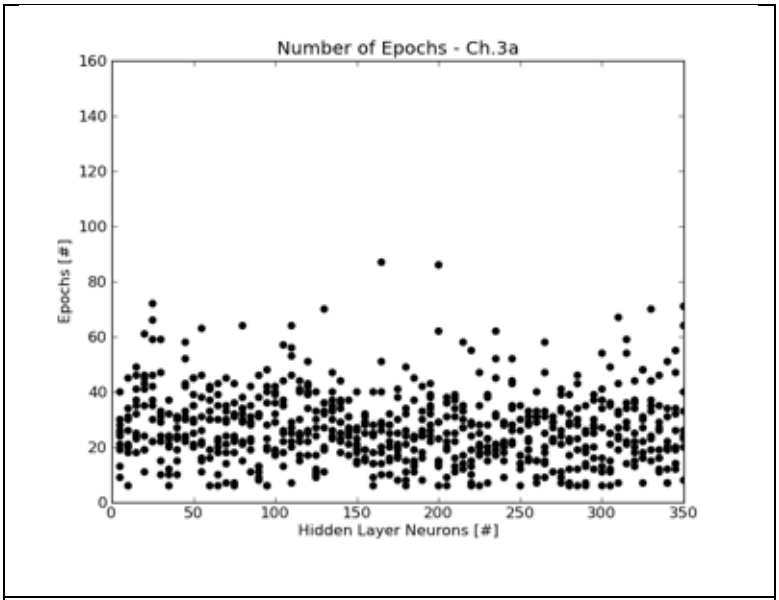

Figure B3 – Number of training epochs required using AVHRR data from Ch.3a.

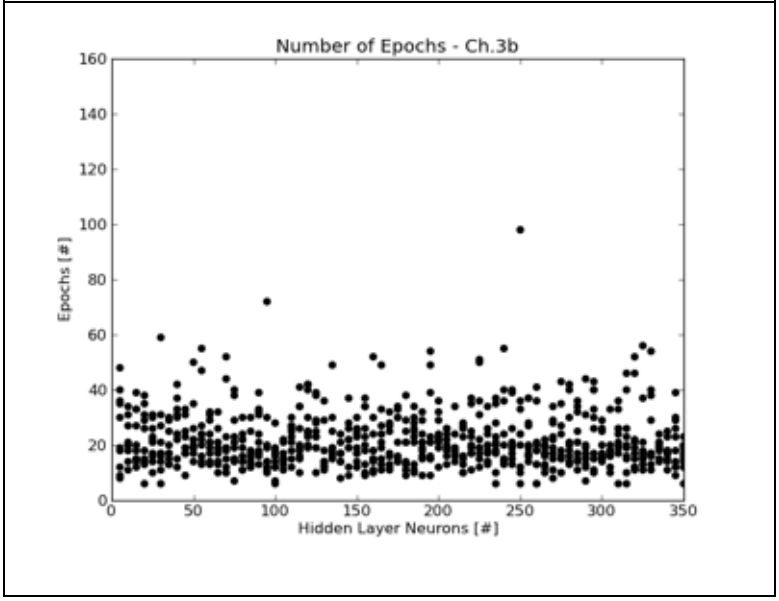

Figure B4 – Number of training epochs required using AVHRR data from Ch.3b.

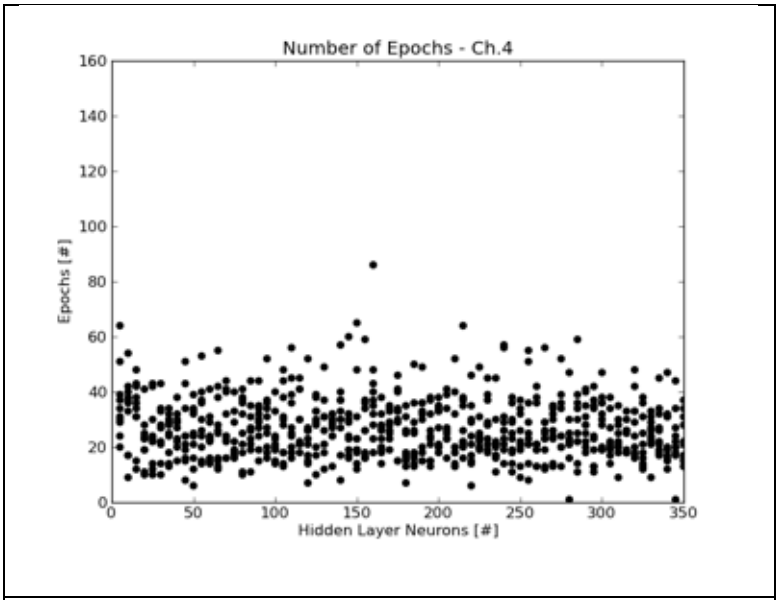

Figure B5 – Number of training epochs required using AVHRR data from Ch.4.

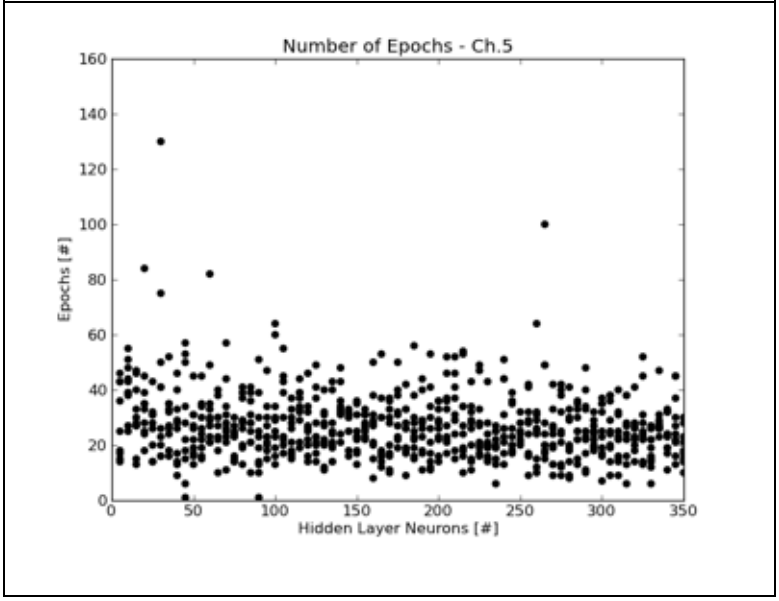

Figure B6 – Number of training epochs required using AVHRR data from Ch.5.

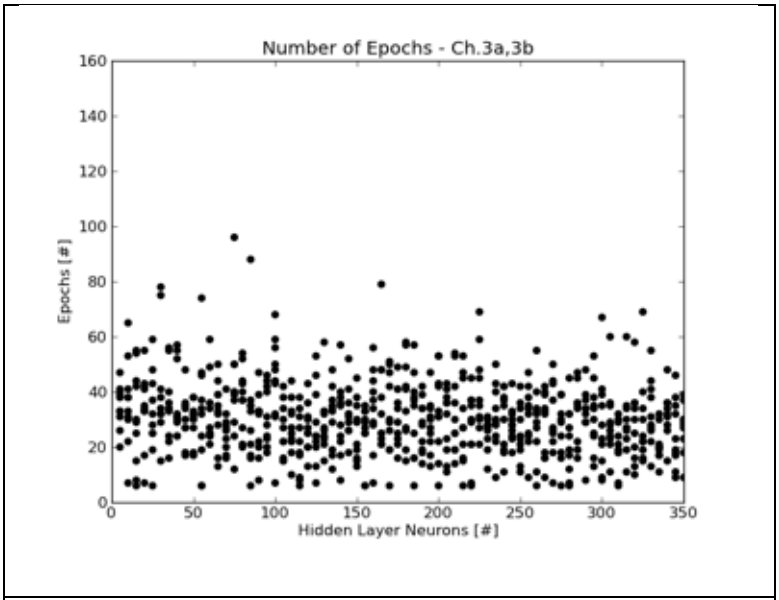

Figure B7 – Number of training epochs required using AVHRR data from Ch.3a,3b.

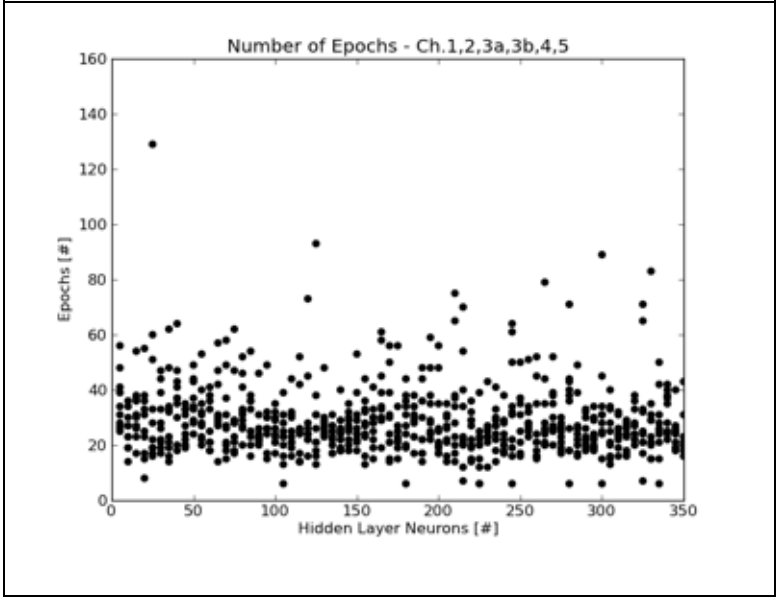

Figure B8 – Number of training epochs required using AVHRR data from all six channels.

Appendix C – Test Data Sub-Set Confusion Parameters

The following plots summarize classification with the standard confusion matrix parameters (false positive, false negative, true positive, true negative) for the test data sub-set. Results for each channel combination are presented.

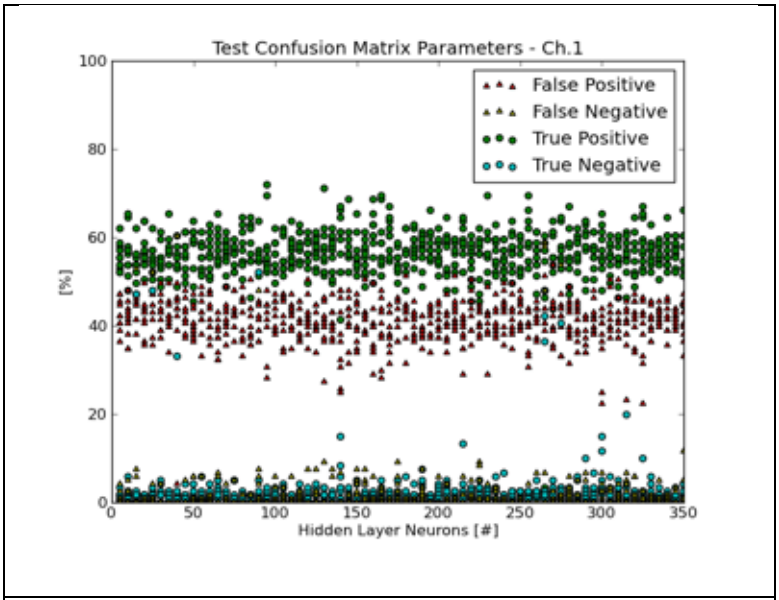

Figure C1 – Confusion matrix parameters for the test data sub-set using AVHRR data from Ch.1.

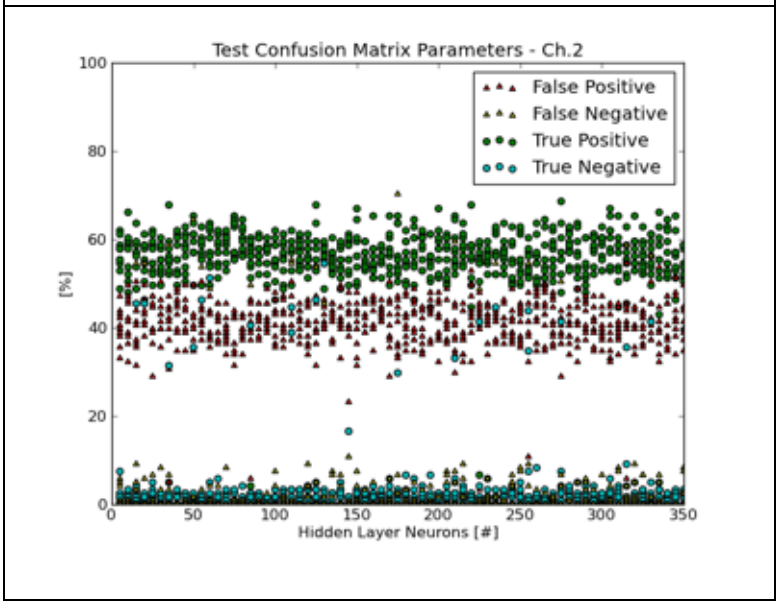

Figure C2 – Confusion matrix parameters for the test data sub-set using AVHRR data from Ch.2.

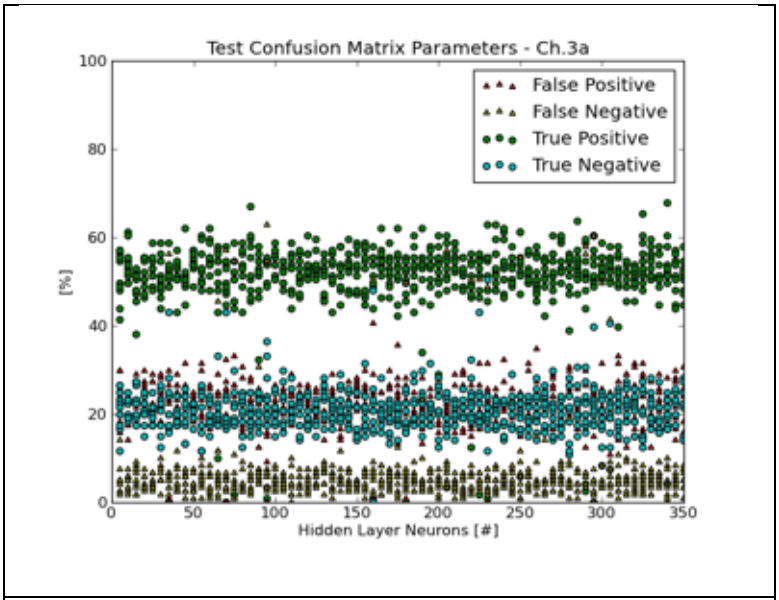

Figure C3 – Confusion matrix parameters for the test data sub-set using AVHRR data from Ch.3a.

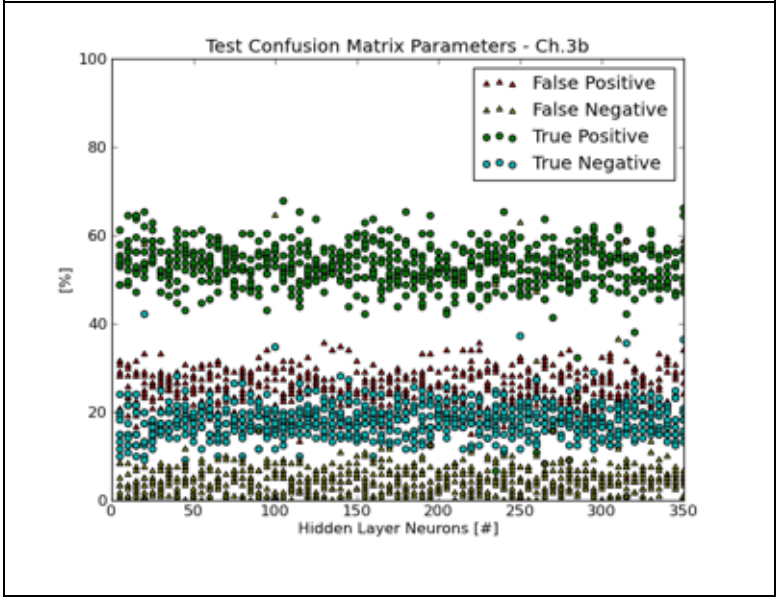

Figure C4 – Confusion matrix parameters for the test data sub-set using AVHRR data from Ch.3b.

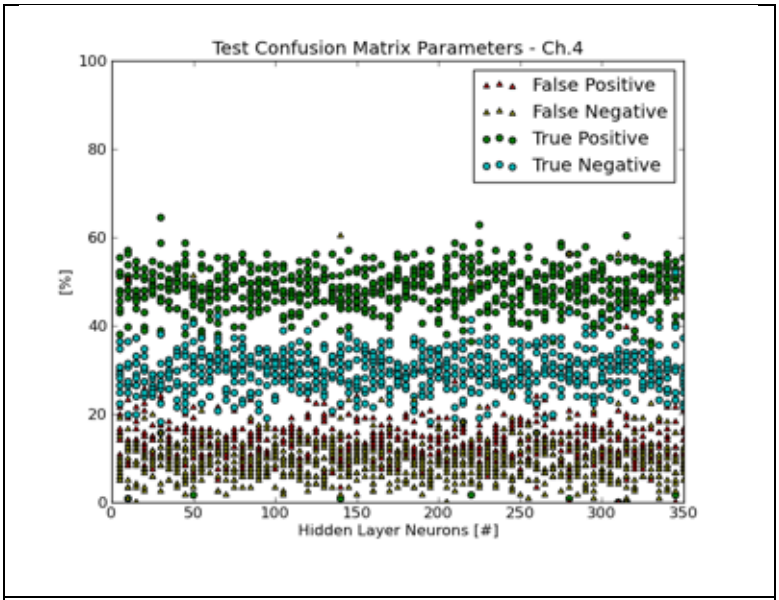

Figure C5 – Confusion matrix parameters for the test data sub-set using AVHRR data from Ch.4.

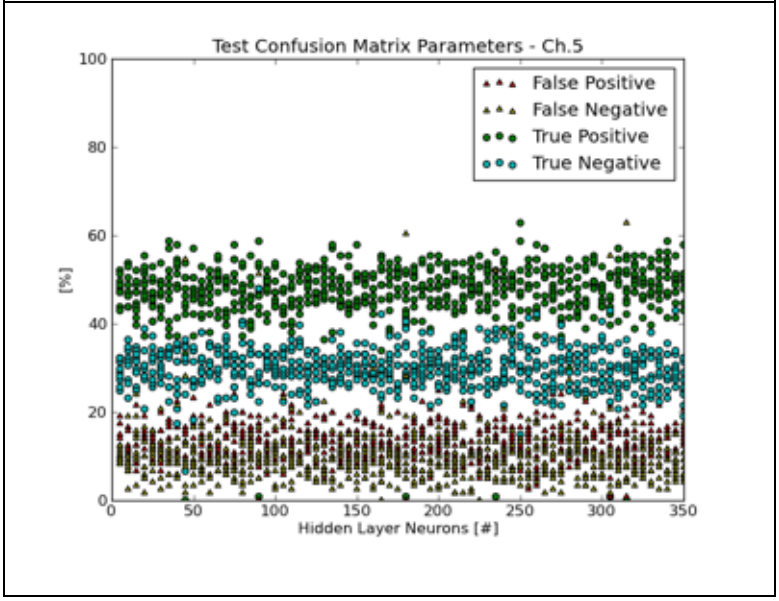

Figure C6 – Confusion matrix parameters for the test data sub-set using AVHRR data from Ch.5.

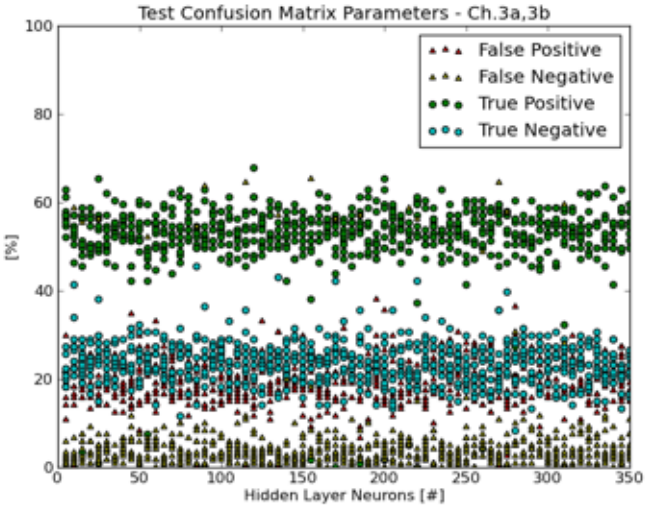

Figure C7 – Confusion matrix parameters for the test data sub-set using AVHRR data from Ch.3a,3b.

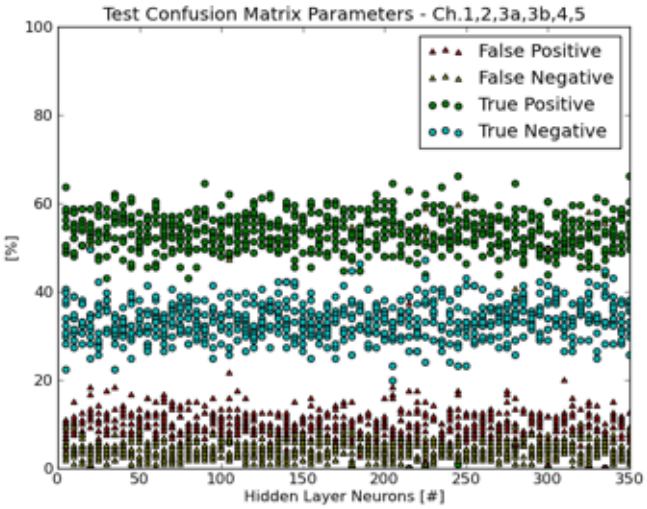

Figure C8 – Confusion matrix parameters for the test data sub-set using AVHRR data from all channels.

Appendix D – Validation Data Sub-Set Confusion Parameters

The following plots summarize classification with the standard confusion matrix parameters (false positive, false negative, true positive, true negative) for the validation data sub-set. Results for each channel combination are presented.

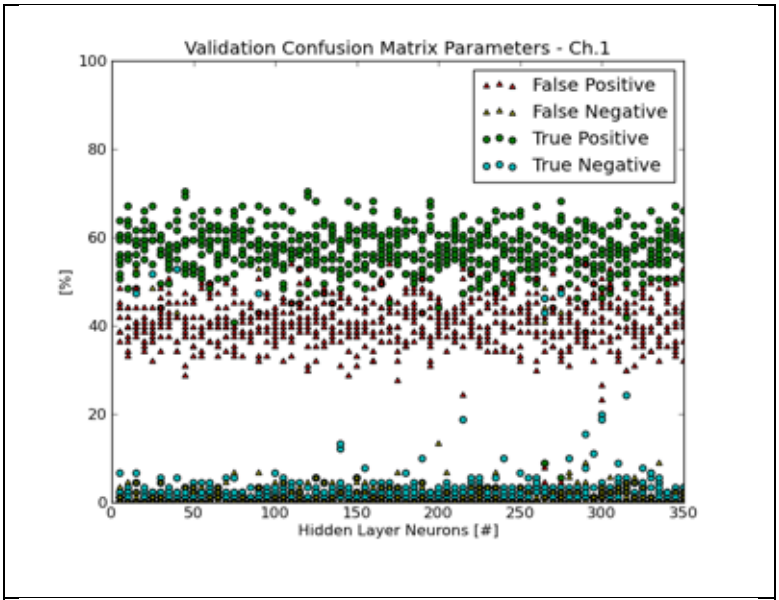

Figure D1 – Confusion matrix parameters for the validation data sub-set using AVHRR data from Ch.1.

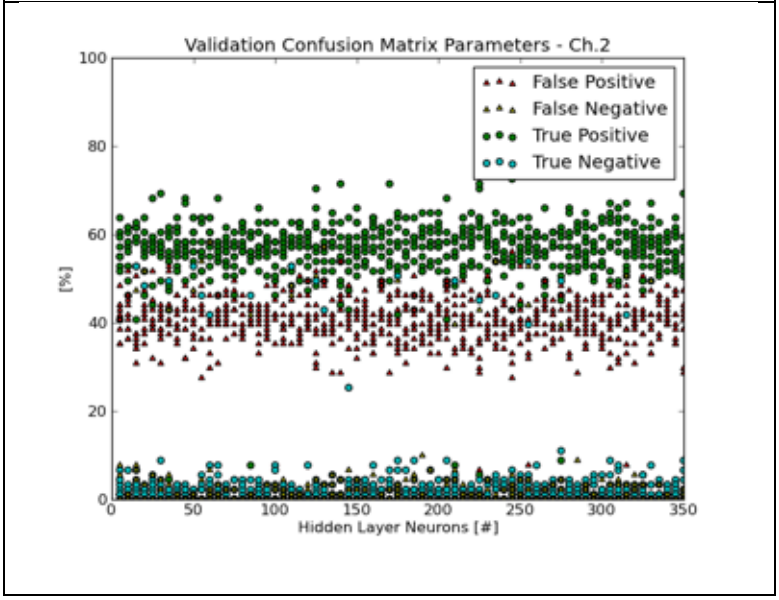

Figure D2 – Confusion matrix parameters for the validation data sub-set using AVHRR data from Ch.2.

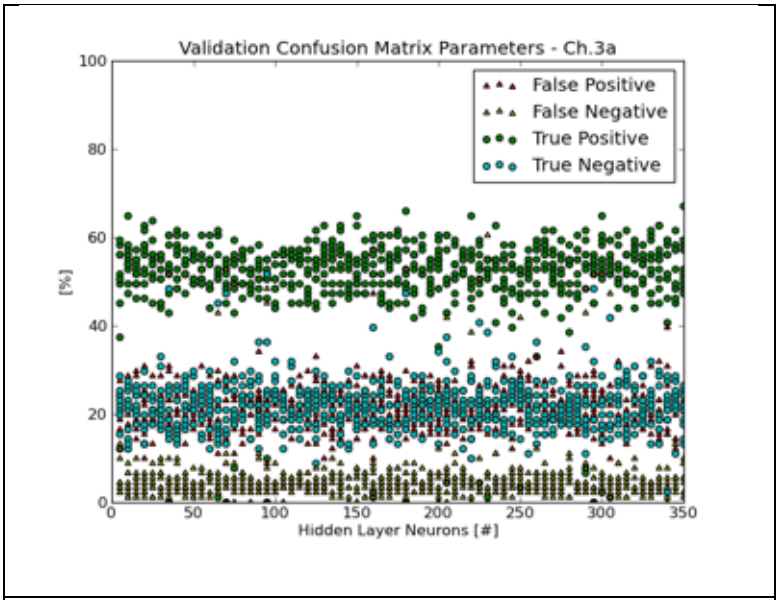

Figure D3 – Confusion matrix parameters for the validation data sub-set using AVHRR data from Ch.3a.

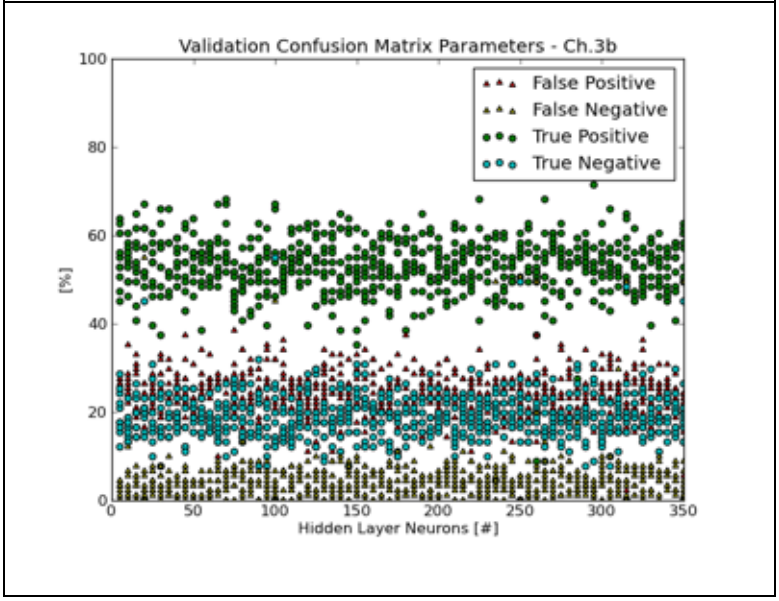

Figure D4 – Confusion matrix parameters for the validation data sub-set using AVHRR data from Ch.3b.

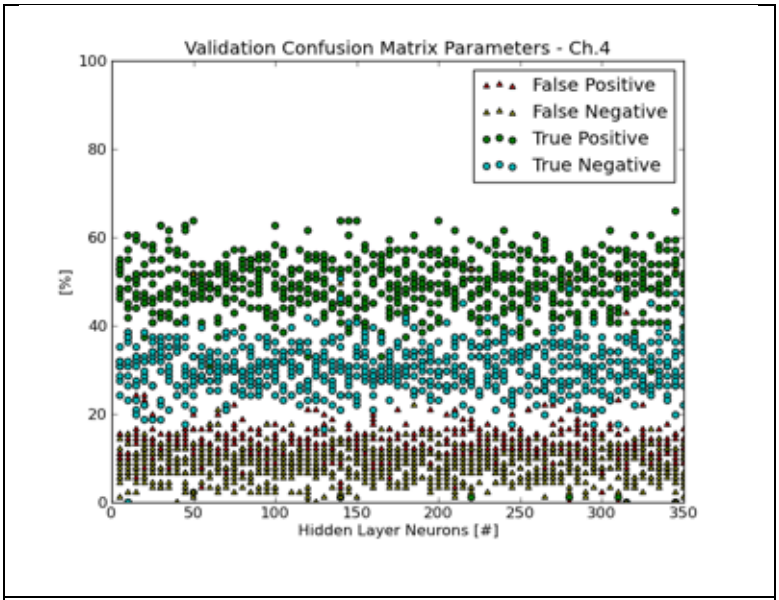

Figure D5 – Confusion matrix parameters for the validation data sub-set using AVHRR data from Ch.4.

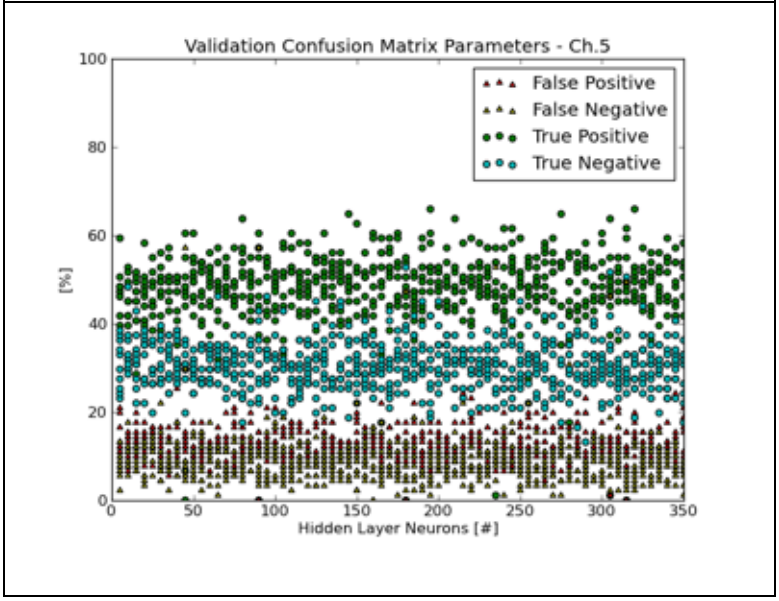

Figure D6 – Confusion matrix parameters for the validation data sub-set using AVHRR data from Ch.5.

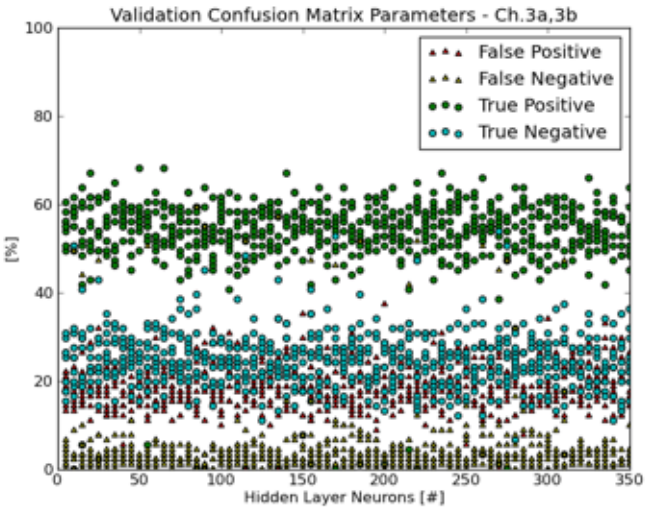

Figure D7 – Confusion matrix parameters for the validation data sub-set using AVHRR data from Ch.3a,3b.

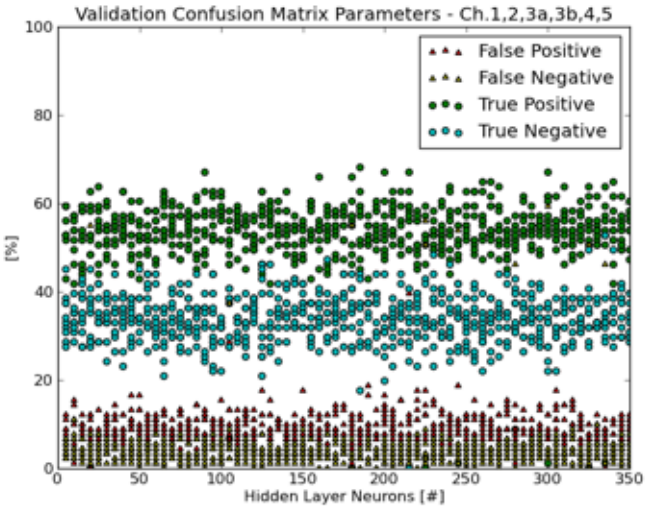

Figure D8 – Confusion matrix parameters for the validation data sub-set using AVHRR data from all channels.

Appendix E – Training Confusion Parameters

The following plots summarize classification with the standard confusion matrix parameters (false positive, false negative, true positive, true negative) for the training data sub-set. Results for each channel combination are presented.

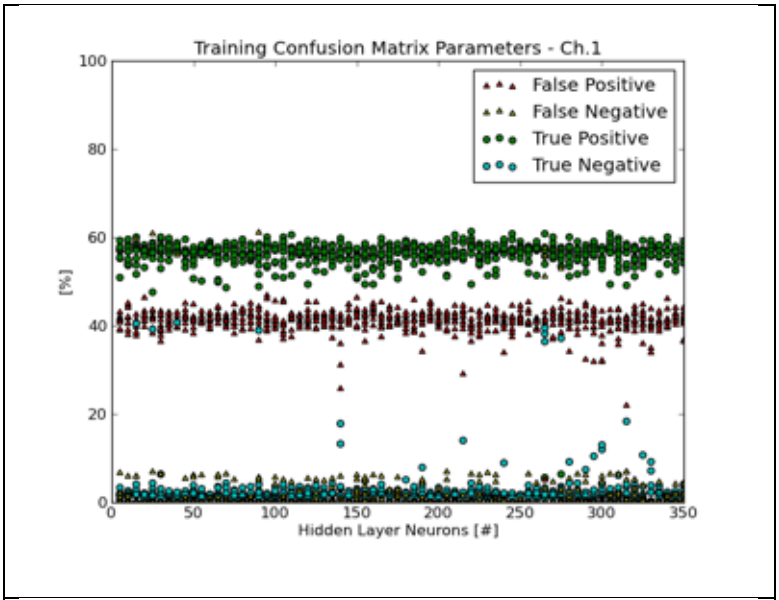

Figure E1 – Confusion matrix parameters for the training data sub-set using AVHRR data from Ch.1.

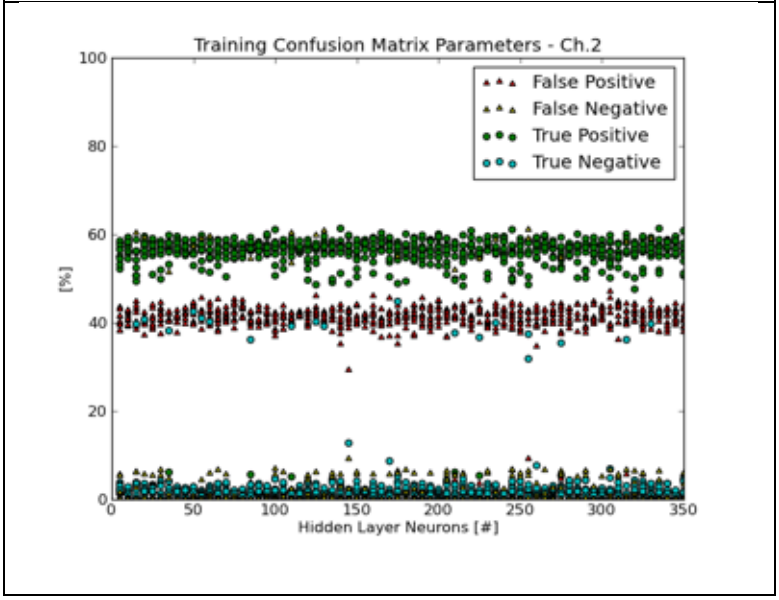

Figure E2 – Confusion matrix parameters for the training data sub-set using AVHRR data from Ch.2.

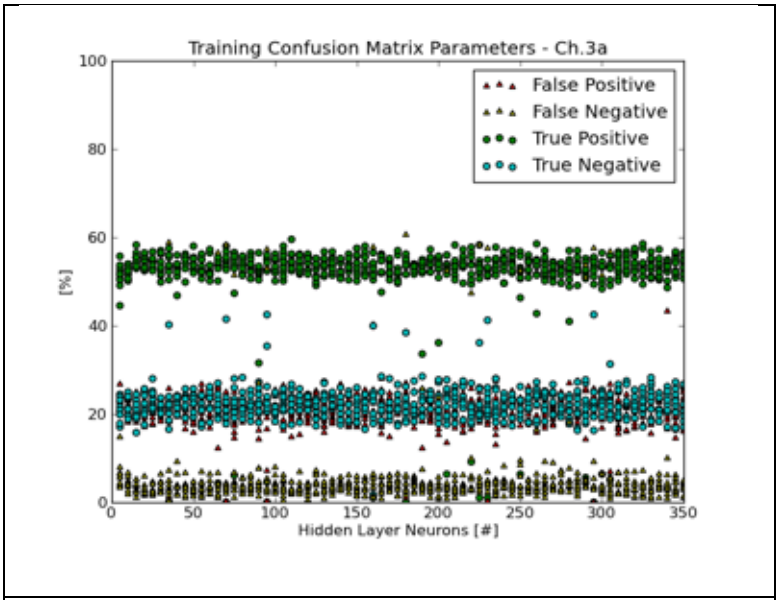

Figure E3 – Confusion matrix parameters for the training data sub-set using AVHRR data from Ch.3a.

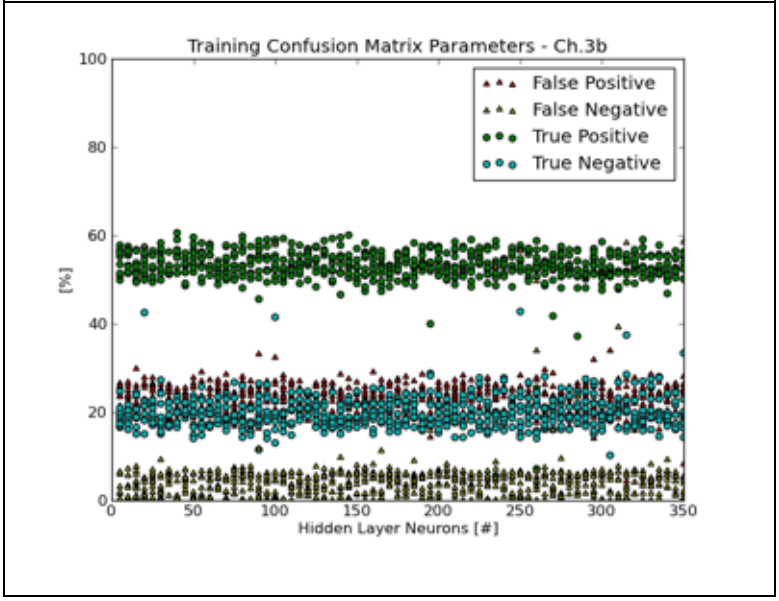

Figure E4 – Confusion matrix parameters for the training data sub-set using AVHRR data from Ch.3b.

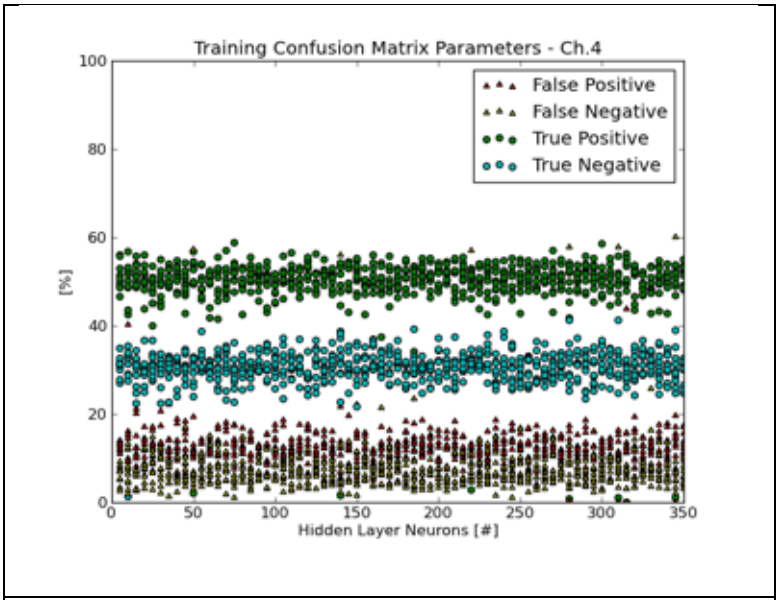

Figure E5 – Confusion matrix parameters for the training data sub-set using AVHRR data from Ch.4.

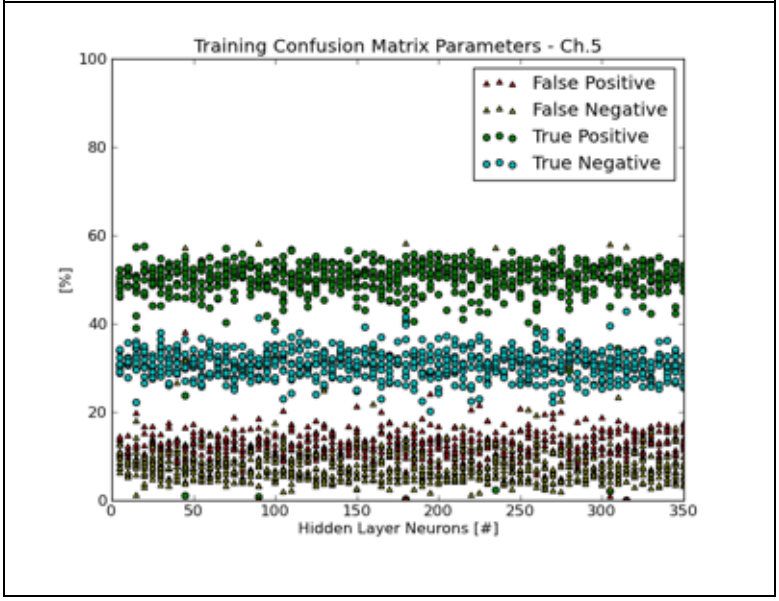

Figure E6 – Confusion matrix parameters for the training data sub-set using AVHRR data from Ch.5.

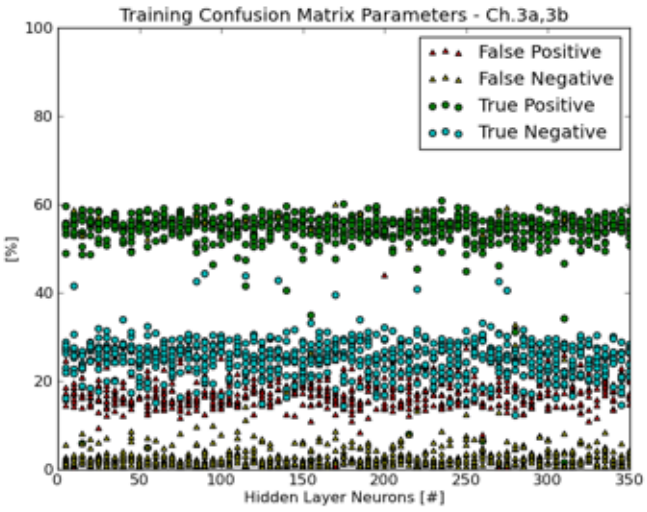

Figure E7 – Confusion matrix parameters for the training data sub-set using AVHRR data from Ch.3a,3b.

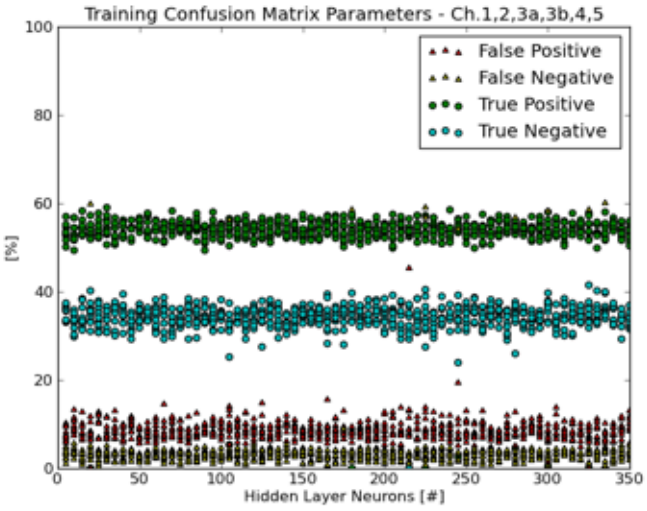

Figure E8 – Confusion matrix parameters for the training data sub-set using AVHRR data from all channels.

Appendix F – Total Confusion Parameters

The following plots summarize classification with the standard confusion matrix parameters (false positive, false negative, true positive, true negative) for all data sub-sets. Results for each channel combination are presented.

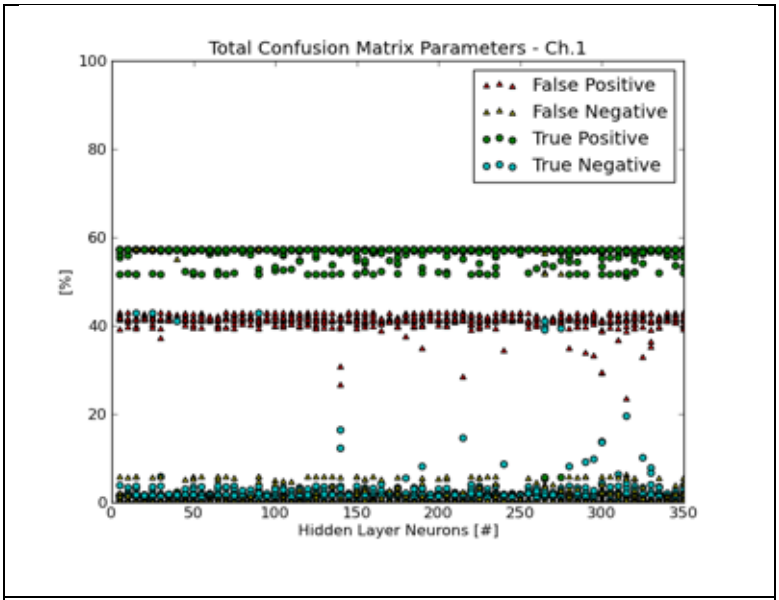

Figure F1 – Confusion matrix parameters for the all data sub-sets using AVHRR data from Ch.1.

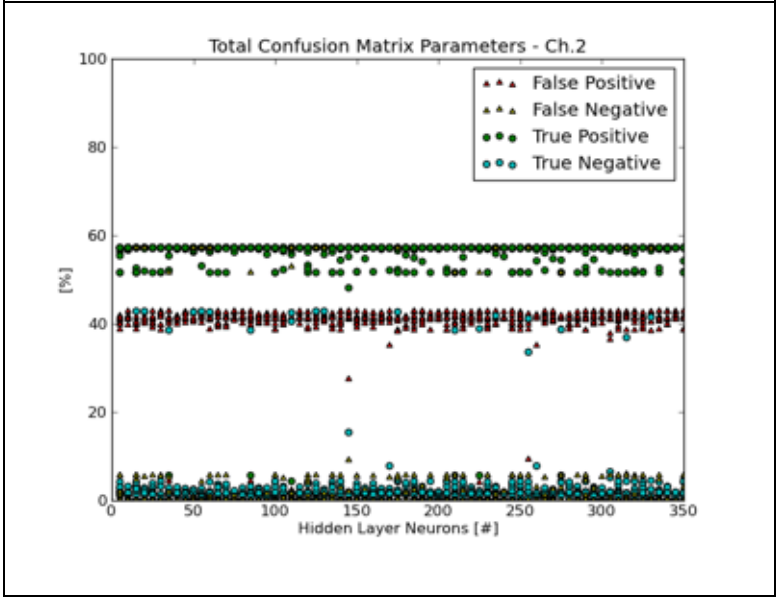

Figure F2 – Confusion matrix parameters for the all data sub-sets using AVHRR data from Ch.2.

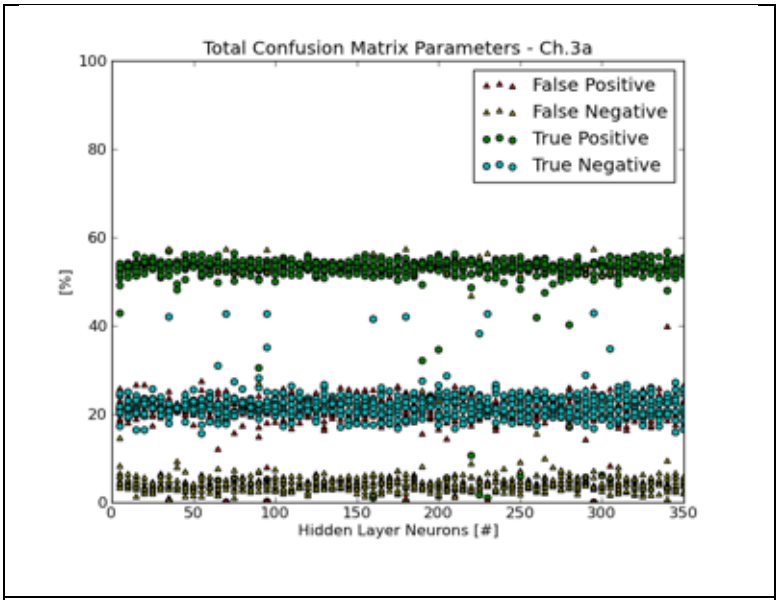

Figure F3 – Confusion matrix parameters for the all data sub-sets using AVHRR data from Ch.3a.

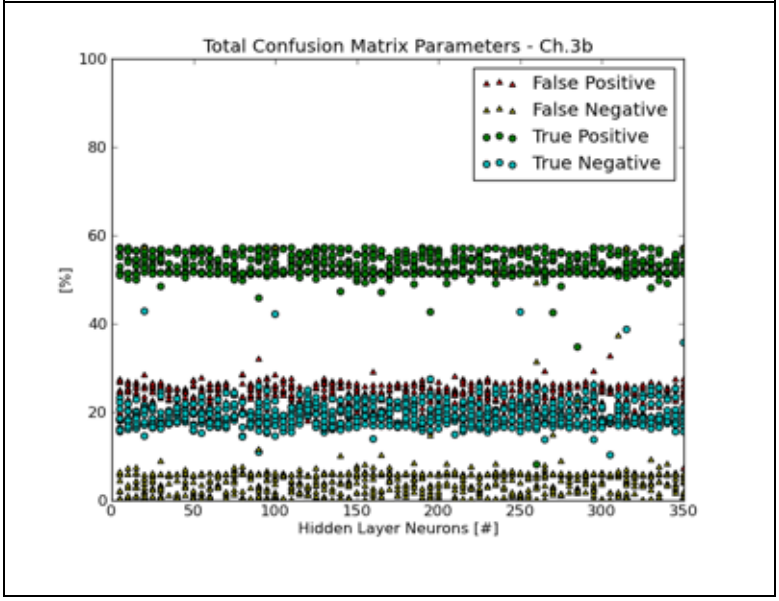

Figure F4 – Confusion matrix parameters for the all data sub-sets using AVHRR data from Ch.3b.

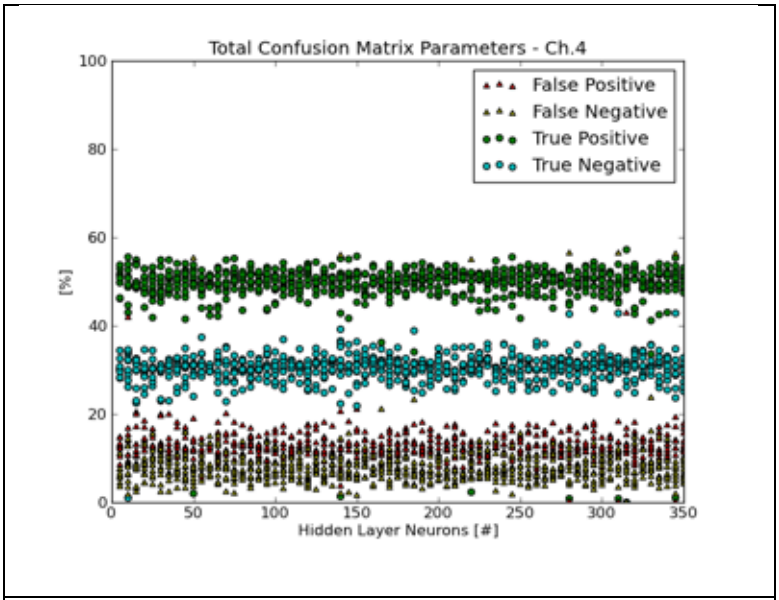

Figure F5 – Confusion matrix parameters for the all data sub-sets using AVHRR data from Ch.4.

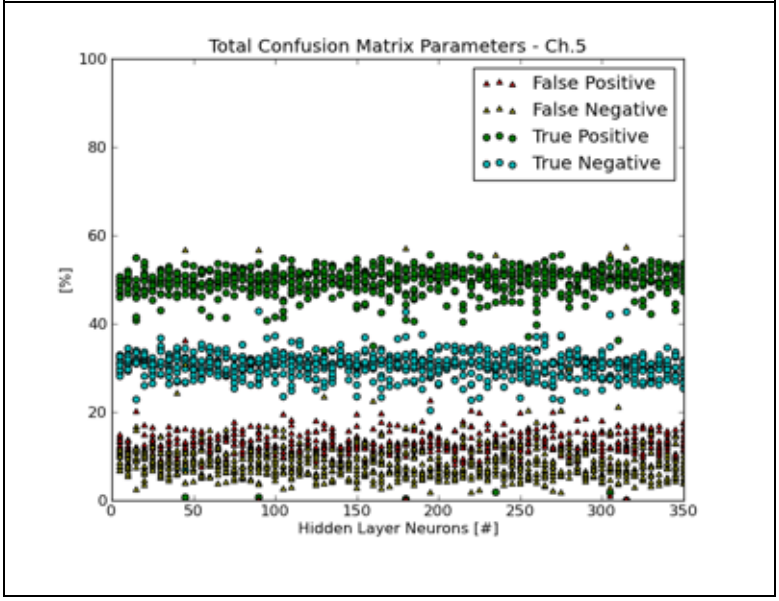

Figure F6 – Confusion matrix parameters for the all data sub-sets using AVHRR data from Ch.5.

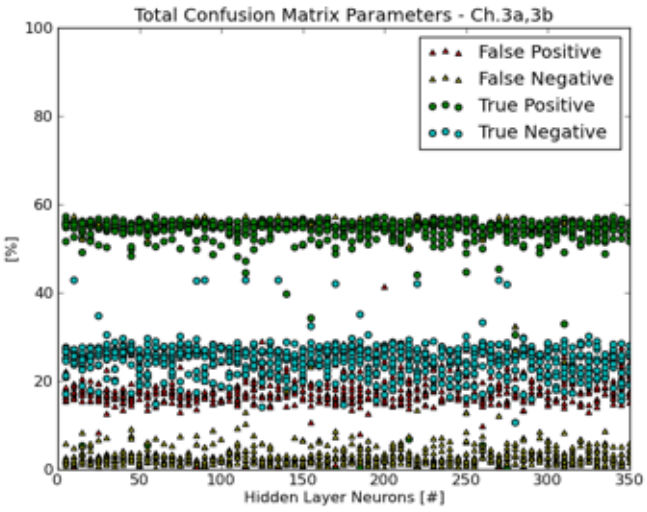

Figure F7 – Confusion matrix parameters for the all data sub-sets using AVHRR data from Ch.3a,3b.

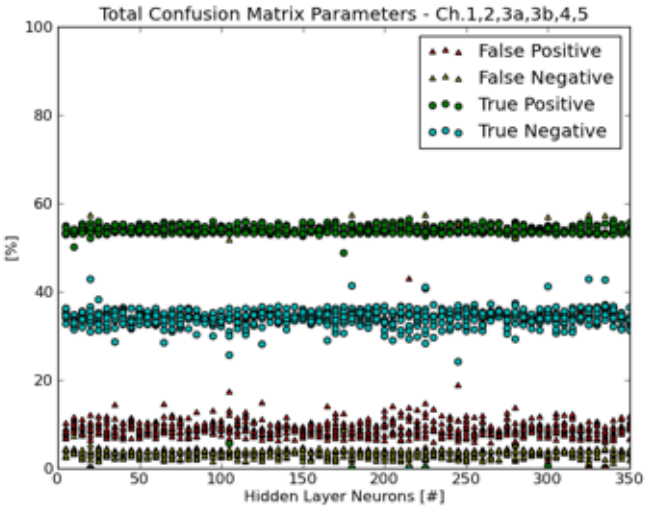

Figure F8 – Confusion matrix parameters for the all data sub-sets using AVHRR data from all channels.

Appendix G – AVHRR Instrument Parameters

A summary of AVHRR parameters from the instrument documentation. Complete documentation available from NOAA or http://oiswww.eumetsat.org/WEBOPS/eps-pg/AVHRR/AVHRR-PG-4ProdOverview.htm

Table G1 – Spectral specifications for the AVHRR.

Channel	Central wavelength (µm)	Half power points (µm)
1	0.630	0.580 - 0.680
2	0.865	0.725 - 1.000
3a	1.610	1.580 - 1.640
3b	3.740	3.550 - 3.930
4	10.800	10.300 - 11.300
5	12.000	11.500 - 12.500

Table G2 – Scanning parameters for the AVHRR.

Characteristics	Value	Unit
Scan direction	East to West (northbound)	-
Scan type	continuous	-
Scan rate	0.025	ms
Sampling interval (duration)	0.1667	s
Sampling interval	0.0541	deg
Pixels/scan	2048	-
Swath	±55.3	deg
Swath width	±1446.58	km
IFOV	0.0745	deg
IFOV type	square	-
IFOV size (nadir)	1.08	km
IFOV size (edge) - across track	6.15	km
IFOV size (edge) - along track	2.27	km
Scan separation	1.1	km